

# We are IntechOpen, the world's leading publisher of Open Access books Built by scientists, for scientists

6,900

Open access books available

186,000

International authors and editors

200M

Downloads

Our authors are among the

154

Countries delivered to

TOP 1%

most cited scientists

12.2%

Contributors from top 500 universities



WEB OF SCIENCE™

Selection of our books indexed in the Book Citation Index  
in Web of Science™ Core Collection (BKCI)

Interested in publishing with us?  
Contact [book.department@intechopen.com](mailto:book.department@intechopen.com)

Numbers displayed above are based on latest data collected.  
For more information visit [www.intechopen.com](http://www.intechopen.com)



## DMF - A New Biofuel Candidate

Guohong Tian, Ritchie Daniel and Hongming Xu  
*University of Birmingham and Newcastle University  
 United Kingdom*

### 1. Introduction

Although there are very few biomass-derived fuels which are competitive to fossil fuels, the scientific research community has never ceased to search for renewable biofuel alternatives. For use in the transportation sector, a practical biofuel must:

- be produced economically and efficiently;
- have a relatively high energy density, in both volume and weight, in order to achieve competitive mileage;
- be easy to store and distribute;
- have sufficient reserves, which do not threaten ecosystems;
- be sourced from a variety of bio-mass or bio-waste;
- have suitable properties for use in existing power generation systems without the need for major modifications.

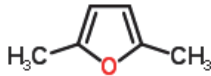

Most potential biofuels meet the majority of these requirements. However, none satisfies them all, not even the most successful gasoline-alternative biofuel, bio-ethanol. Despite its success in the Brazilian market, bio-ethanol requires a large amount of sugar cane, which can put stress on food production and the environment.

Hitherto, little has been able to compete with bio-ethanol, that is until the production techniques of 2,5-dimethylfuran, known as DMF, were significantly improved (Yuriy Roman-Leshkov 2007; Zhao H 2007). These advances have sparked interest in the research community to investigate the adaptability of this new biofuel candidate to be used in power generation systems, particularly in internal combustion engines.

### 2. What is DMF?

DMF, a derivative of furan, is a heterocyclic compound with the formula  $(\text{CH}_3)_2\text{C}_4\text{H}_2\text{O}$ . Its main properties are listed in Table 1. In order to better understand the relative strength of DMF, the corresponding properties for bio-ethanol (referred to as ethanol in this Chapter) and gasoline are also listed in the table.

As shown in the table, DMF has several advantages over ethanol as a gasoline-alternative biofuel. Firstly, the gravimetric energy density, or lower heating value, of DMF is approximately 1/3 higher than ethanol, much closer to that of gasoline, which improves mileage for the same size of fuel tank. In terms of volume, the lower heating value of DMF is less than 10% lower than gasoline and over 40% higher than ethanol. Secondly, unlike ethanol, DMF is insoluble in water, which makes it easier to store. Thirdly, DMF has a

Name(s)	2,5 Dimethylfuran 2,5 Dimethyl-furan 2,5 Dimethylfurane 2,5 Dimethyloxole	Ethanol Ethyl Alcohol Ethyl Hydroxide EtOH	Gasoline Petrol
CAS Registry Number	625-86-5	64-17-5	8006-61-9 86290-81-5
Linear Structure Formula	$(CH_3)_2C_4H_2O$	$CH_3OCH_3$	Variable
Molecular Formula	$C_6H_8O$	$C_2H_6O$	$C_2$ to $C_{14}$
Molecule Schematic			Variable
M, Molecular Mass	96.1289g/mol <sup>1</sup>	46.069g/mol <sup>1</sup>	100 – 105g/mol <sup>2</sup>
Type of Substance	Heterocyclic	Acyclic	Aliphatic Hydrocarbon Mixture
Appearance	Colorless Liquid	Colorless Liquid	Colorless to amber colored liquid
Aroma	Spicy, Smokey	Vinous	Petroleum odor
Safety	Flammable, Irritant	Flammable, Irritant, CNS effects	Highly Flammable, Irritant
Water Solubility <sup>3</sup>	Insoluble <1mg/ml @73°F	Highly soluble >=100mg/ml @73°F	Insoluble
MP, Boiling Point (1atm)	–62.8°C <sup>3</sup>	–130°C <sup>4</sup>	-
BP, Boiling Point (1atm) <sup>1</sup>	93.0°C	77.3°C	96.3°C(FBP)
Enthalpy of Vaporization (20°C) <sup>4</sup>	31.91kJ/mol	43.2496kJ/mol	-
Enthalpy of Formation <sup>5</sup>	–97.9kJ/mol @298.15K	–234.963kJ/mol	-
Vapor Pressure	7.2 kPa (22°C) <sup>6</sup>	7.869 kPa(25°C) <sup>7</sup>	72.007 kPa4(25°C)
ρ, Density of Liquid	895.4kg/m <sup>3</sup> @20°C	793.63kg /m <sup>3</sup> @15°C	-

1 Beilstein Database April 2008  
2 US Department of Energy. Alternative Fuels and Advanced Vehicles Data Centre. October 2008  
3 Cameo Chemicals, US Gov. Chemical Data Sheet, 2, 5 Dimethylfuran. October 2008  
4 Chemspider.com January 2009 (NB: Prediction Software is utilised by this source when experimental values are unavailable)  
5 F M WELLE & Others. Thermochemical Studies for Determination of the Standard Molar Enthalpies of Formation of Alkyl-Substituted Furans and Some Ethers. Structural Chemistry June 1998  
6 NTP, 1992  
7 <http://www.iterasi.net/openviewer.aspx?sqrilitid=qpgkevc0qugba9dhaqnsyw>

Vapor Density (air=1)	3.31 <sup>7</sup>	1.59 <sup>8</sup>	3-4 <sup>9</sup>
Refraction Index (20°C) <sup>4</sup>	1.443	1.361	-
Specific Gravity (4°C, 1atm) <sup>4</sup>	0.892-0.898	0.910	-
Molar Volume (4°C, 1atm) <sup>4</sup>	104.7cm <sup>3</sup>	59cm <sup>3</sup>	-
Surface Tension <sup>4</sup>	25.9dyne cm	22.3dyne cm	20dyne cm <sup>-1</sup>
Polar Surface Area <sup>4</sup>	13.14Å <sup>2</sup>	9.23Å <sup>2</sup>	-
Viscosity (1atm, 20°C)	0.65cP <sup>10</sup>	1.2cP <sup>11</sup>	0.4-0.5cP <sup>12</sup>
Research Octane Number (RON)	-	110 <sup>2</sup>	95 <sup>13</sup>
Heat of Vaporization	332 kJ/kg	840 kJ/kg	373 kJ/kg
Lower Heating Value	33.7MJ/kg	26.9MJ/kg	42.9MJ/kg

Table 1. Main properties of DMF, benchmarked with ethanol and gasoline

higher boiling point, which makes it less volatile and more practical as a liquid fuel for transportation. Fourthly, DMF has a similar heat of vaporisation to gasoline, which will help to overcome the difficulty of cold starts seen with ethanol. Finally, and most attractively, DMF is completely uncompetitive with food and potentially more energy efficient to produce.

Although DMF has been used as an octane improver for gasoline, it has served other purposes. Before being considered as an alternative fuel, DMF was used in the food industry with a low production efficiency and high cost. However, new production techniques have been reported by a group of biochemists at the University of Wisconsin-Madison in the US, who published their work in Nature, in 2007 (Yuriy Roman-Leshkov 2007). Here, the authors claimed a new development that allows the mass production of DMF from bio-mass with low energy consumption and high yield. Figure 1 shows the rationale for converting these carbohydrates to DMF. As described in the publication, five oxygen atoms need to be removed from a hexose, for example, fructose to produce DMF. The selective removal can be accomplished in two steps: first, by removing three oxygen atoms through dehydration to produce 5-hydroxymethylfurfural (HMF); and second, by removing two oxygen atoms through hydrogenolysis to produce DMF by the way of the following intermediates: 2-methyl,5-hydroxymethylfuran and 2-methylfuran (4 and 5 in Figure 1)(Yuriy Roman-Leshkov 2007).

8 Material Safety Data Sheet, Ethanol, Absolute. <https://fscimage.fishersci.com/msds/89308.htm>

9 GASOLINE SAFETY. [http://www.burnsurgery.org/Documents/gasoline\\_safety.doc](http://www.burnsurgery.org/Documents/gasoline_safety.doc)

10 knovel database

11 <http://en.wikipedia.org/wiki/Ethanol>

12 <http://chemed.chem.purdue.edu/genchem/topicreview/bp/ch14/property.php>

13 Delphi. Worldwide Emissions Standards, Passenger Cars & Light Duty Trucks. 2008

Shortly after their publication, this concept was further developed by Zhao and his co-workers, who observed high yields of HMF (the intermediate for DMF; see Figure 1), without the need for acid catalysts (Zhao H 2007). Not only does Zhao's method dramatically reduce the production costs, it also includes glucose as a potential feedstock for HMF. Furthermore, Mascal reported that cellulose itself can be converted into furanic products (Mascal 2008). Such advances have attracted attention towards DMF as a potential gasoline-alternative biofuel (Luque 2008).

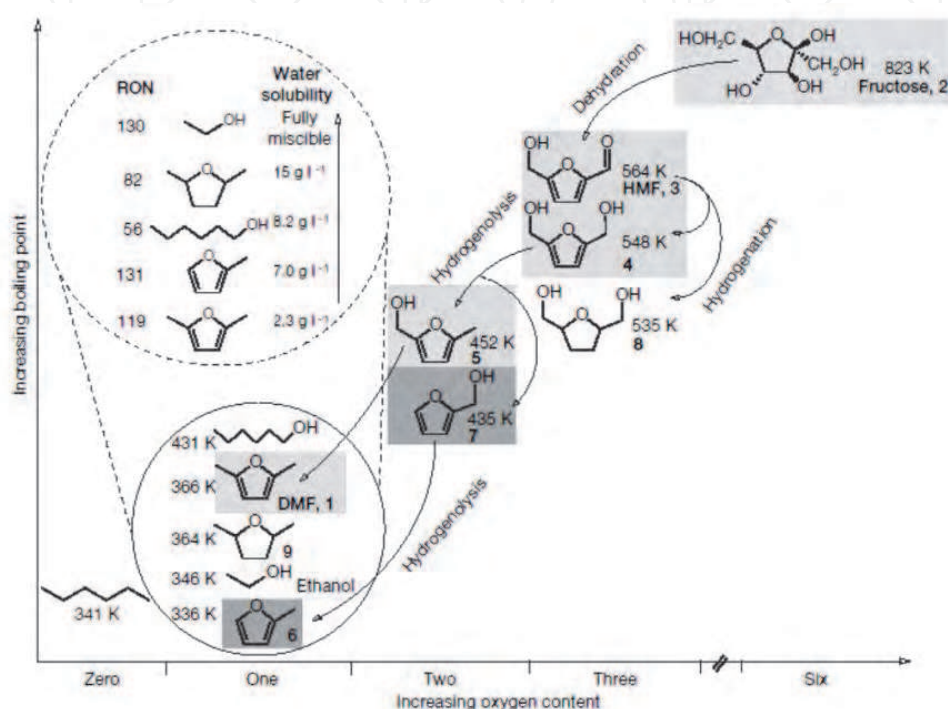


Fig. 1. The rationale for converting carbohydrates to DMF(Yuriy Roman-Leshkov 2007)

The success of the biochemists triggered a quick response from the automotive research community. Engineers were interested in the adaptability of DMF as an alternative automotive fuel. The research was firstly initiated at Birmingham University in the UK to investigate its combustion performance and emissions as an alternative fuel in modern automotive engines. The portfolio of work covers several key aspects of internal combustion engine science. This includes the spray characteristics, laminar burning velocity, engine performance, regulated and unregulated engine emissions and some novel methods for optimising the use of biofuels. Xi'an Jiaotong University in China has also reported a series of studies on the burning behaviour of DMF(Xuesong Wu 2009).

### 3. Spray characteristics

Fuel spray characteristics are essential to engine performance and emissions, particularly for direct-injection engines. The initial factors include the injection pressure, injector design, and fuel properties. They directly influence the fuel-air mixture generation and consequently, combustion behaviour. Optical methods, utilising shadowgraph and high-speed cameras, are often used to measure the main spray characteristics with time, including the spray cone angle and penetration length. For more advanced engine designs,

the behaviour of such parameters as the fuel droplet size and velocity distribution are preferred. The information can be measured accurately by advanced laser based measurement techniques, e.g. Phase Doppler Particle Analyser (PDPA, also known as Phase Doppler Anemometry, PDA). This information can be used to understand the environmental impact of the spray development in order to help the design of injection and combustion systems. At the same time, such details can supplement computational simulation models, which can help to refine the engine design process.

A group of shadowgraph spray images from a multi-hole injector at different injection timings is shown in Figure 2. The images were cut in order to focus on one spray. The injection pressure in the fuel rail was 10MPa and the injection duration was set to 2ms. The first spray image was captured 0.8ms after the injection trigger, slightly longer than the 0.7ms solenoid response time for the specific injector used for the test. This method clearly shows the spray development with time, where the penetration length reached over 70mm at 2ms after the start of injection. It also shows a leaner spray at the injection tip due to the evaporation of the fuel droplets. This information is very helpful for the design and optimisation of injectors and combustion chambers, in order to prevent any fuel impingement on the cylinder wall or piston bowl, which is likely to increase the unburned hydrocarbon emissions. However, the information obtained from the image is limited and more comprehensive techniques are needed to provide more details of the injection pattern.

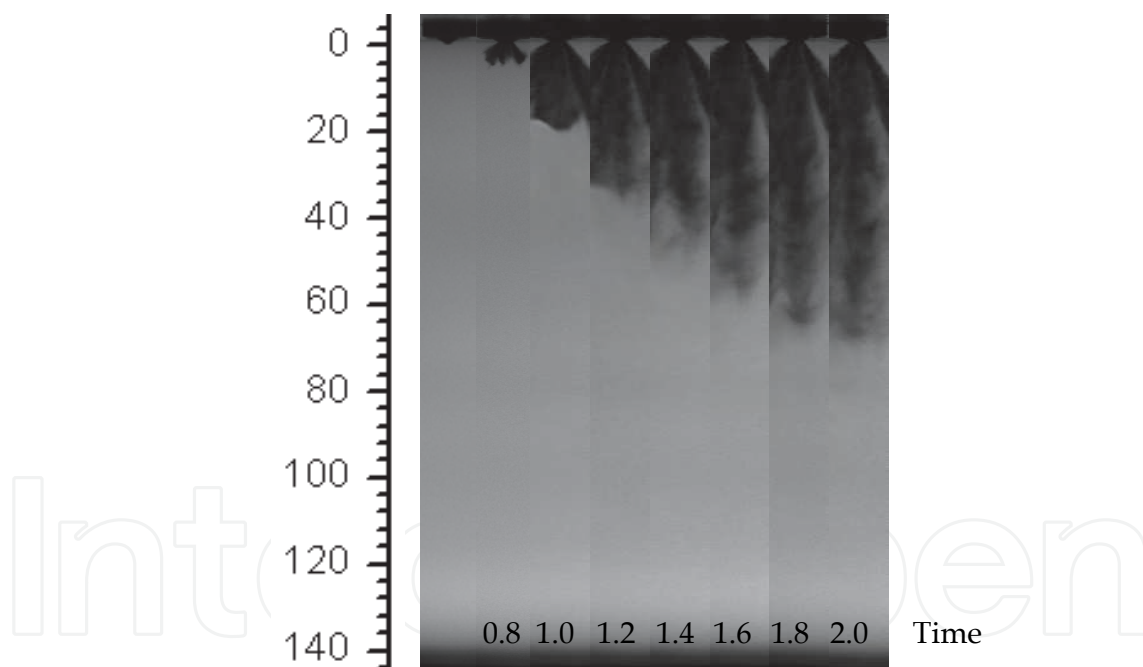


Fig. 2. Shadowgraph images for DMF spray (injection pressure: 100MPa, length unit: mm, time unit: ms)

PDPA is an advanced laser-based technology used to measure liquid droplet size and velocity distribution. It gives statistical information for a high number of droplets ( $>10^4$ ) by obtaining the size and velocity information for each droplet passing through the microscopic measuring point. It normally takes hundreds of injections to gather a sufficient number of validated droplets at one point. With the results from different positions in the spray, a spray map with detailed size and velocity information can be provided to better describe the spray. This helps the comprehensive understanding of the spray characteristics.



A typical PDPA measurement result (velocity) at one test point is illustrated in Figure 3. Each point represents a single measured droplet, where, in this figure, there are over 15,000 droplets. For a clearer comparison between the different fuels, a smooth profile was averaged over 0.05ms time intervals. The curve clearly indicates the spray structure and therefore the trend of velocity development.

The spray structure can be arbitrarily divided into two parts: spray 'head' and 'tail', which are marked in the figure. In the spray head, the droplets have a relatively high velocity with a low deviation. However, in the spray tail, the mean velocity drops quickly until it reaches a minimum. In this case, 1.1ms after the start of injection (ASOI), the spray head reached the measuring point and the droplets were captured. The delay consists of two parts: the solenoid response time, which is approximately 0.7ms (for this injector), and the spray travelling time. The highest velocity of the droplets was 80m/s and the lowest was 20m/s approximately, which gives a wide velocity distribution range. The droplet generation process can explain this phenomenon. The first stage of this process includes the liquid filament breakup (after injection) due to the shearing force between the air and the spray envelope. Resultantly, these droplets slow down and are hit by the ensuing droplets, causing their trajectories to rapidly change. As a result, the real velocity of the ensuing droplets with unchanged trajectories is higher than those with changed trajectories. After the spray head has passed, several droplets with much lower velocity reach the measuring volume (recognized as the 'tail' of the spray). This results in the negative velocity of some droplets which could induce vortices caused by the pressure gradient of the surrounding gas. Several low velocity droplets were captured before and during the spray head. These droplets are believed to be the residual droplets from the previous injection and were ignored due to the negligible quantity.

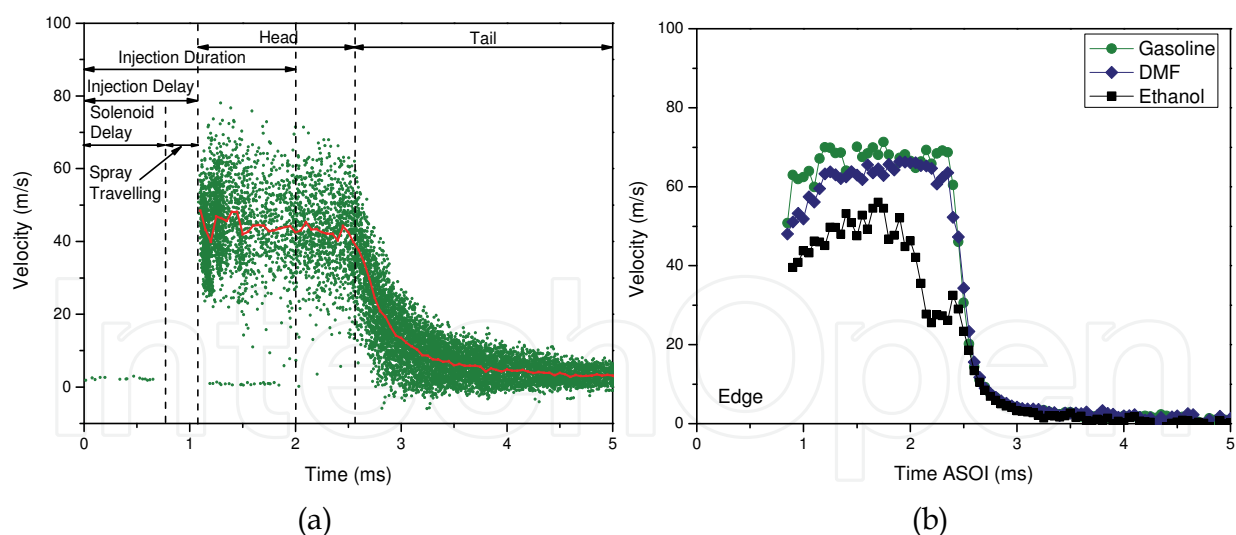


Fig. 3. (a) Typical PDPA measured velocity distribution (tested fuel: benchmarking gasoline, injection pressure: 10MPa, measure position: 32mm downstream from nozzle at the axle) and (b) mean velocities of tested fuels (measure position: 8mm downstream from nozzle at the edge of spray)

Although the test results shown in Figure 3 are only from one velocity vector, juxtaposing the data of DMF with gasoline and ethanol helps to understand the behaviour of the fuel. These results show the great similarity of DMF and gasoline in terms of droplet velocity.

However, ethanol was observed to have an overall lower velocity distribution at all test points, as highlighted by the example in Figure 3 (b). In fact, DMF and gasoline have very close physical properties, which play a major role in the spray characteristics.

The droplet size distribution is normally more useful than the velocity information, since it gives direct information about how liquid fuels break up, evaporate and generate the desired fuel-air mixture. Statistical values, such as the Sauter Mean Diameter (SMD), are widely used in computational simulation models. The formula to calculate the SMD is as follows:

$$D_{32} = \frac{\sum N_i d_i^3}{\sum N_i d_i^2} \quad (1)$$

As a multiple test point approach, PDPA is capable of giving droplet size information at all test points. The SMD maps for the three test fuels have been drawn out by this means and are shown in Figure 4. As discovered by other researchers, all three test fuels have larger droplets close to the nozzle than downstream and closer to the middle than at the edge.

For all the test fuels, the droplet size decreases rapidly soon after the fuel was injected. After 24mm downstream of the spray, the droplet sizes become stable, which can be explained by the secondary break-up process. The break-up lengths of the three fuels are also similar. Primary break-up cannot be detected by this method due to the high density of droplets which can be considered filaments and not necessarily droplets.

For gasoline, a slight increase in droplet size along the axis can be observed, but not for DMF or ethanol. Further than 40mm from the nozzle, no significant difference was observed in terms of droplet size between the gasoline and DMF sprays. However, the ethanol spray behaves differently. Near the nozzle, the ethanol droplets are the smallest of the three fuels. However, the ethanol spray conversely has the largest droplets downstream. The SMD variation of ethanol along the axis (16.9-20.2 $\mu$ m) is lower than for the other two fuels (16-22.5 $\mu$ m and 14.9-23.4 $\mu$ m, for gasoline and DMF, respectively).

The stable droplet size is mainly affected by three physical properties; vapor density, surface tension and relative velocity. According to Chu's theory (Chu 1986), the stable droplet size is proportional to the surface tension, inversely proportional to the vapor density and square of the relative velocity. DMF, ethanol and gasoline have similar surface tensions (25.9, 22.3 and 20dyne/cm, respectively, see Table 1). However, ethanol has the lowest vapor density at 1.59 (relative to air, see Table 1), which, according to the theory (Chu 1986), is why ethanol has the largest stable droplet size. Nevertheless, this theory cannot explain why ethanol has the smallest droplet size near the nozzle. It can be assumed that ethanol has the shortest primary break-up length, which means at the same position away from the nozzle, more droplets break-up in the ethanol spray than in the other two. However, more research is required to fully support this hypothesis.

Another issue is the effect on the SMD of the injection pressure. As shown in Figure 5, the SMDs of DMF, ethanol and gasoline were measured at the same arbitrary sampling point with injection pressure variations from 50bar to 150bar, thus covering most modern direct-injection spark-ignition applications. Generally, the higher the injection pressure, the smaller the SMD becomes. Within the tested pressure region, the profile shows good linearity. The SMD for gasoline and DMF behave similarly. At 50bar, the SMD for both gasoline and DMF are around 21 $\mu$ m and decrease in unison to 13 $\mu$ m at 150bar. Ethanol, once again, performs differently. With increasing injection pressure, the SMD of the ethanol droplets reduces at a lower rate. At 15MPa injection pressure, Ethanol has an SMD more than 15 $\mu$ m, which is 2 $\mu$ m higher than gasoline.



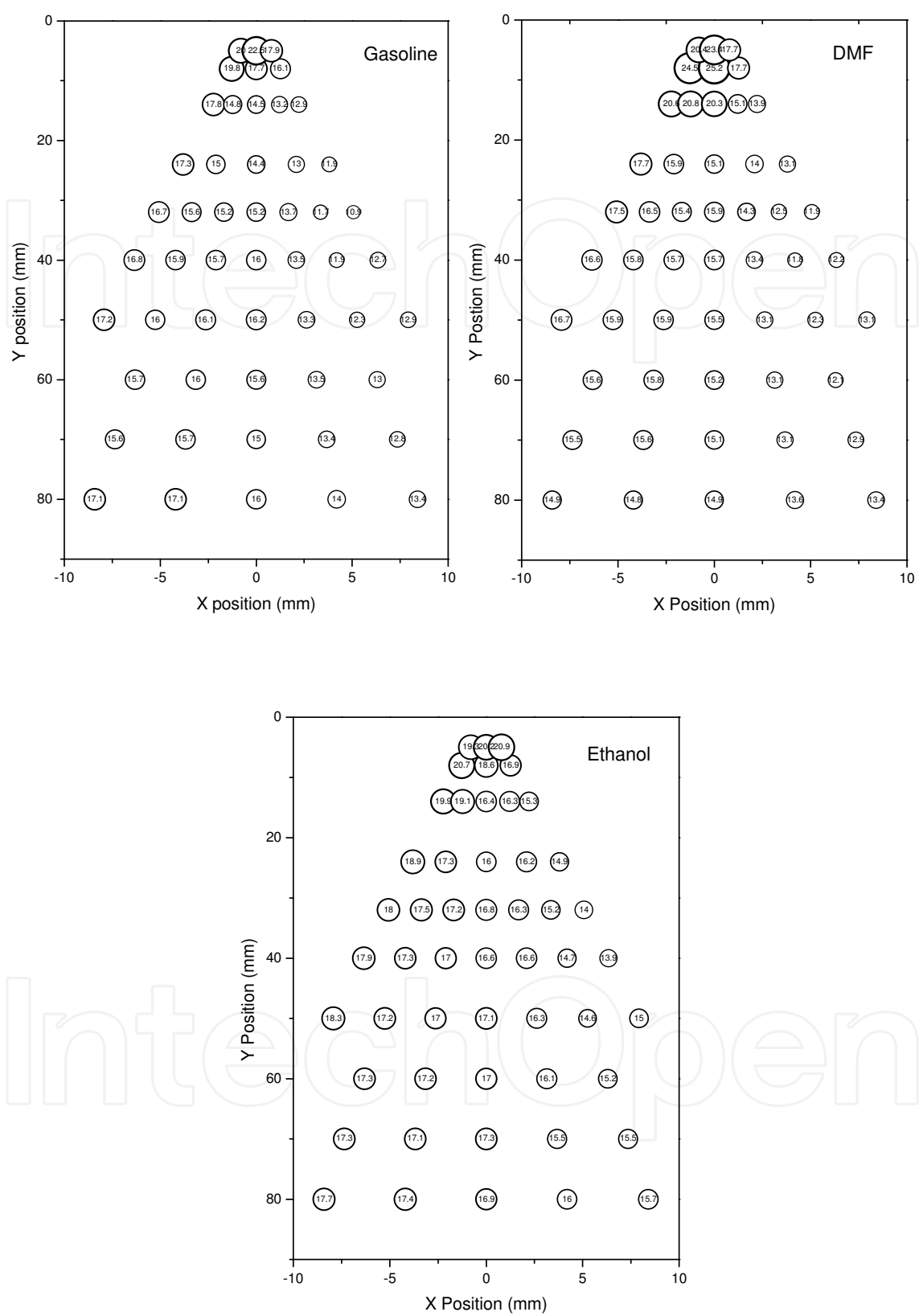


Fig. 4. SMD maps for gasoline, ethanol and DMF (Injection pressure: 10MPa, injection duration: 2mm)

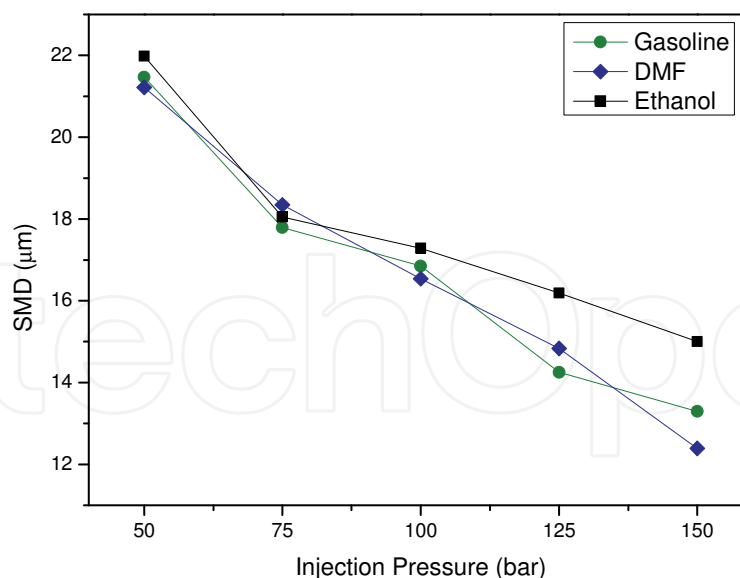


Fig. 5. Effect on injection pressure on SMD (sampling point: 32mm downstream of nozzle on axis)

In summary, the spray characteristics of DMF are particularly favourable. The spray pattern when using DMF is very similar to that with gasoline. Although the DMF spray has a marginally lower velocity than with gasoline, the competing biofuel, ethanol, has a significantly lower velocity in the spray head region and a higher rate of reduction compared to the others. The DMF spray also has a negligibly larger droplet size than the gasoline spray, while ethanol has more abundant droplets. These findings highlight DMF's suitability to match gasoline's behaviour and so would not require major modifications to the fuel injection system.

#### 4. Laminar burning velocity

Laminar burning velocity is another important fuel characteristic and is necessary for simulation work. For phenomenological combustion models, a complete understanding of the chemical kinetics of the flame reactions is required. However, due to the complexity and stochastic nature of turbulence, most numerical models rely on the experimental laminar burning velocity to interpret the turbulent component. In fact, the laminar burning velocity directly affects the burn rate and thus the engine performance. Different methodologies are available to study the laminar burning velocity. A widely used technique is to study premixed quiescent combustion, such as that in a constant volume vessel. In this method, a spherical flame develops from initial spark energy and propagates outwardly. The laminar flame speed is then interpreted using high-speed photography. As the product mass in the vessel increases, the pressure and unburned gas temperature upstream of the flame increase as well. However, as this methodology necessitates steady-state ambient conditions, only the data sampled before the increase of pressure and temperature can be used for data analysis (empirically when the spherical flame diameters are smaller than 10% of the vessel inner diameter).

Schlieren techniques are one of the most commonly used optical access methods, due to the cost effectiveness, accuracy and simplicity. The Schlieren method captures images with varying density gradients found at the flame front during combustion. A typical Schlieren test bench plan is presented in Figure 6.

The well established premixed combustion theory will not be discussed here. However, several basic concepts of laminar flame propagation are helpful to understand the following discussion. The concepts will be limited to the case of quiescent premixed combustion with outwardly propagating spherical flames (Law 2006).

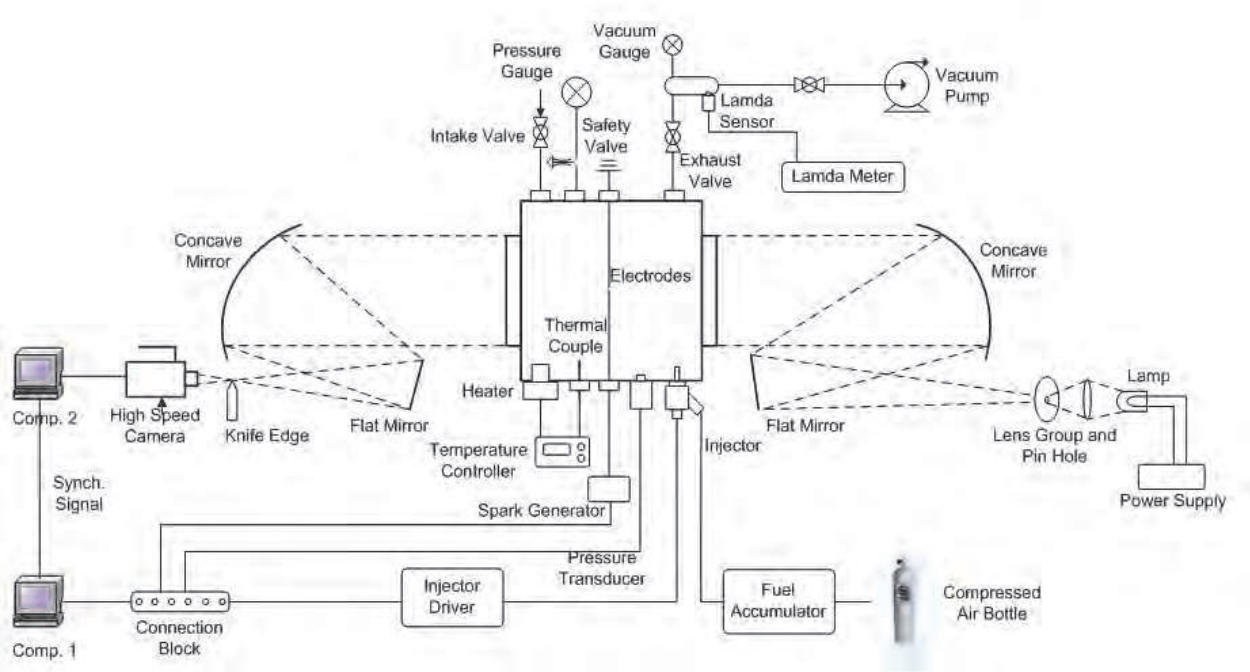


Fig. 6. Schematic of Schlieren test setup

Stretch rate: the flame curvature has a strong influence on the structure and thus the flame speed measurement. The intensity of stretch is represented by a stretch rate,

$$\alpha = \left( \frac{2}{r_f} \right) \left( \frac{dr_f}{dt} \right) \tag{2}$$

with units  $s^{-1}$ , where  $r_f$  is the measured spherical flame radius.

Stretched flame speed: the direct measurement of the flame front propagation speed is defined as:

$$S_n = \frac{dr_f}{dt} \tag{3}$$

Therefore, the stretch rate is:

$$\alpha = \frac{2}{r_f} S_n \tag{4}$$

Unstretched flame speed: the downstream flame speed is significantly affected by the stretched flame and can be shown to be approximately linear to the stretch rate. This linearity allows the extrapolation of the stretched flame speed to the zero stretch rate, where we can obtain the unstretched flame speed  $S_s$ .

Markstein length: the Markstein length,  $L_b$ , is determined by the negative slope of the line when extrapolating the stretched flame speed to the zero stretch rate:

$$S_n = S_s - L_b \cdot \alpha$$

(5)

This indicates the influence of stretch rate on the flame propagation speed and characterizes the diffusion-thermal instability. Positive Markstein lengths indicate that the flame is stable to the diffusion-thermal effect, while a negative Markstein length indicates that the flame surface is distorted by the diffusion-thermal effect, which leads to flame speed acceleration and the onset of cellularity in the flame surface. According to the research from Bradley et al. (Bradley 1998), if the Markstein number exceeds 1.5, the flame is initially stable until a critical flame radius is reached.

Laminar burning velocity: the laminar burning velocity  $u_l$  is deduced from the unstretched flame speed  $S_s$  using the equation:

$$u_l = S_s \frac{\rho_b}{\rho_u}$$

(6)

where  $\rho_b$  and  $\rho_u$  are the burned and unburned gas densities respectively. The pressures are assumed constant in order to find them via the conservation of mass equation:

$$\frac{\rho_b}{\rho_u} = \frac{V_u}{V_b} = \frac{n_u T_u}{n_b T_b}$$

(7)

where  $n_b$  and  $n_u$  are the mole numbers of the products and reactants, and  $T_b$  and  $T_u$  are the adiabatic flame and initial temperatures, which can be inferred.

Figure 7 juxtaposes three groups of high-speed schlieren images chronologically for DMF, ethanol and gasoline. The images show the stoichiometric ( $\lambda=1$ ), premixed combustion under a pressure of 0.1MPa and temperature of 75°C and are indexed by the time after ignition.

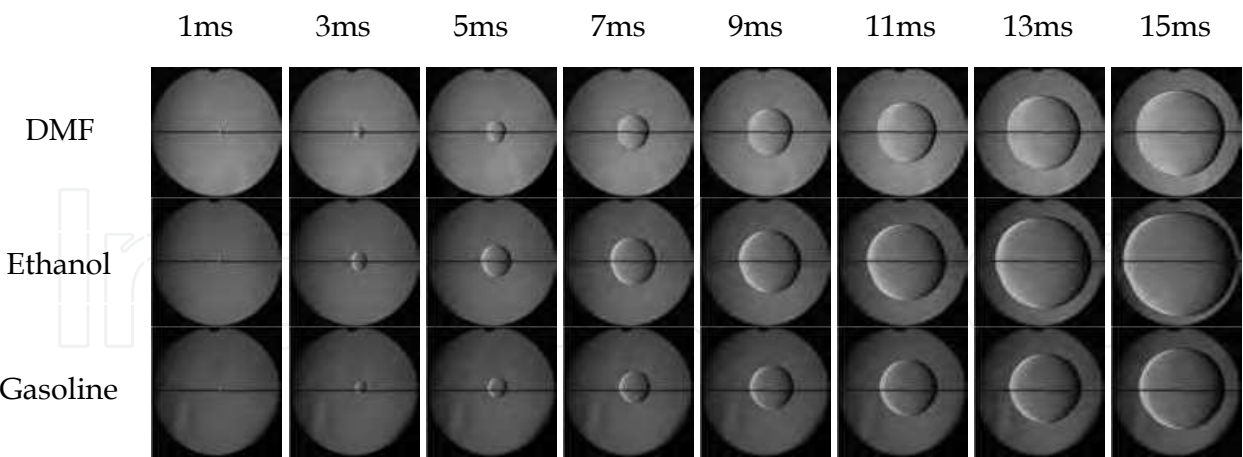


Fig. 7. High speed Schlieren images of DMF, ethanol and gasoline laminar flame propagation

The flame speed when using ethanol is clearly the highest; the relatively advanced flame front, which is established after 3ms, is maintained throughout the expansion. There is very little difference between the cases of DMF and gasoline.

The initiation of the gasoline flame shows the effect of the instability of the spark energy. This is shown between 3 and 5ms, where the flame begins to propagate above the electrode gap. In the DMF and ethanol cases, the centre of the spherical flame is much closer to the

gap and produces a more even distribution relative to the window. As a consequence of the quenching at the electrode-flame interface, the lower flame surface of gasoline develops a crack. However, as the flame develops, it grows evenly in all radial directions. Therefore, by restricting the analysis region to radii greater than 6mm (up to 18mm, approximately 10% of the vessel inner diameter), the influence of the spark instability can be ignored.

The DMF flame propagates evenly in all radial directions; the surface appears smooth and is therefore stable. However, as with the other flames, slight wrinkling is observed near the electrode due to the quenching effect, but this does not affect the overall shape. When the spherical flame approaches the edge of the window, the shape becomes distorted. This effect can be observed more clearly on the ethanol flame after 15ms, as it has reached the most advanced stage. The shape of the flame becomes more oval with flatter vertical surfaces. This is believed to be related to the instability of buoyancy and the influence of the internal geometry of the combustion chamber. From the ethanol flame images, a slight crack is also observed after 5ms, which is believed to be caused by the influence of the electrode.

The stretched flame speed is described as the rate of change of the schlieren flame radius. In order to avoid the impact of the spark energy and the pressure increase in the vessel, only specific images (6mm diameter to 1/10 of the vessel inner diameter, as described previously) were used for the analysis. Figure 8 shows the stretched flame speed of DMF under various equivalence ratios, benchmarked with ethanol and gasoline. The stretched flame speeds were plotted against the stretch rate. The further the flame propagates, the greater the radius and the smaller the stretch rate become. Therefore, with respect to time, the points move towards the zero stretch rate. Through linear extrapolation, both the unstretched flame speed,  $S_u$ , and the Markstein lengths,  $L_b$ , can be determined at the zero stretch rate using the negative slope of the line, shown in Figure 9.

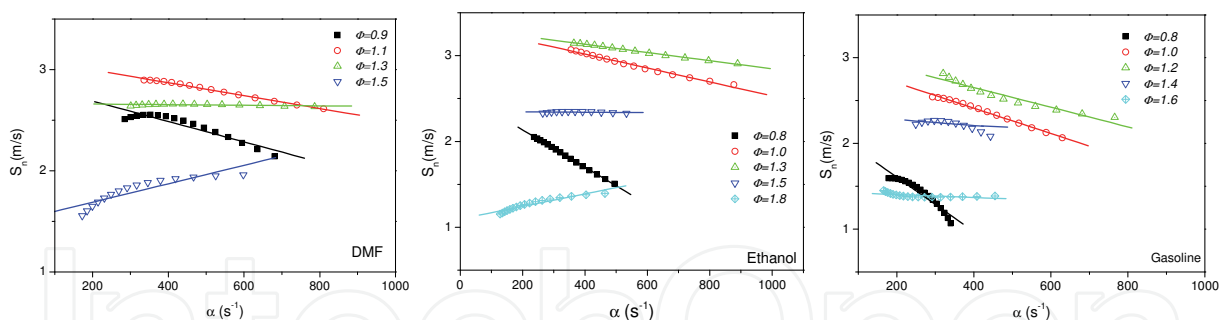


Fig. 8. Stretched flame speed of DMF, benchmarked with ethanol and gasoline (initial temperature: 75°C, pressure: 0.1MPa)

Generally, the Markstein lengths decrease with increasing equivalence ratio, or  $\phi$  ( $\lambda^{-1}$ ) for each initial temperature. This is because the test fuels are heavy hydrocarbon-air mixtures, and the Markstein length depends only on the Lewis number of the deficient reactants (Bechtold 2001).

With regards to temperature, the Markstein lengths have increased at low equivalence ratios (0.8 – 0.9) when the temperature increased. This suggests the flames are much more stable at higher temperatures. However, at high temperature the Markstein lengths then decrease more rapidly from these higher values, suggesting the stability quickly decays. This is also shown by the earlier entry into negative Markstein lengths, with respect to the equivalence ratio, for all three fuels. This indicates that at higher temperatures, the fuel-air mixtures tend



to be more diffusion-thermal unstable and the flame is more susceptible to accelerate with increasing stretch rate. The onset of cellular activity would be quicker and cracks in the flame surface would occur more easily. The rapid decay results in lower Markstein lengths at rich equivalence ratios.

With the exception of 75°C, the ethanol flame appears to be the most stable through the entire range of air-fuel mixtures. However, the difference is insignificant. The Markstein lengths of the DMF flame, on the other hand, are always lower than these of the ethanol flame and partly so for the gasoline flame for this temperature range. This suggests that the DMF flame is slightly more unstable.

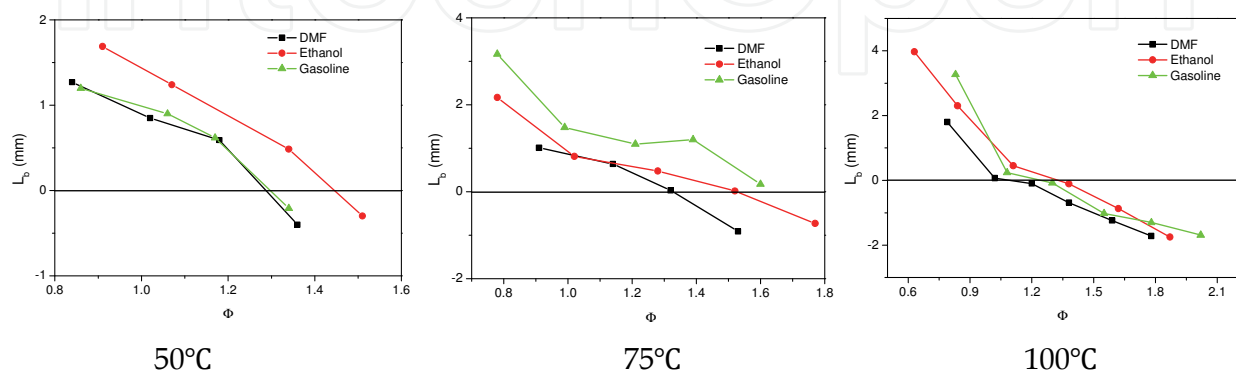


Fig. 9. Markstein lengths of DMF, ethanol and gasoline at various initial temperatures

The Markstein length normally decreases with increasing initial pressure for heavy hydrocarbon fuels. This means at higher initial pressures, the flame propagation is less affected by the flame stretch rate and the flames are less stable, especially for rich mixtures. Figure 10 illustrates the schlieren images at different initial pressures from 0.1MPa to 0.5MPa for a rich mixture ( $\phi=1.2$ ). The fuel used in this test was 20% DMF blended with 80% iso-octane, by volume. For the initial pressures of 0.1 and 0.25MPa, the flame front was smooth without cracks, even when the flame radius reached 30mm. However, at the initial pressure of 0.5MPa, cracks appeared on the flame front when the flame radius was only 10mm. These cracks develop into a cellular structure when the flame radius approaches 30mm under this condition. This is due to the combined effect of diffusional-thermal and hydrodynamic instabilities. The Markstein length and the flame thickness decrease with initial pressure. The increased hydrodynamic instability cannot be reduced by the decreased diffusional-thermal stability.

The aforementioned results can be used to deduce the laminar burning velocities, one of the key indicators of flame behaviour. Figure 11 shows the results for the three fuels for a range of initial temperatures. It is clear that ethanol has the highest burning velocity amongst the three fuels for all the initial temperatures. For instance, at 50°C, the peak laminar burning velocity of ethanol (56cm/s) is 13cm/s higher than that for the gasoline mixture (43cm/s). This difference increases to 17cm/s for 75°C and 15cm/s for 100°C. This reinforces ethanol's superiority, in terms of laminar burning velocity. For the other two fuels, gasoline's laminar burning velocity is more closely matched by DMF, although the laminar burning velocity of DMF is marginally lower. The difference increases as temperature increases and equivalence ratios rise above 1.2. Nevertheless, their profiles are very similar and the curvature is less significant than for ethanol. In real-world engineering applications, e.g. for commercial automotive engines, the equivalence ratios will only slightly deviate around stoichiometric

conditions ( $\Phi=0.9-1.2$ ) due to the requirement of the after treatment system to meet emissions legislations. In this region the difference between the laminar burning velocity of DMF and gasoline is less than 10%.

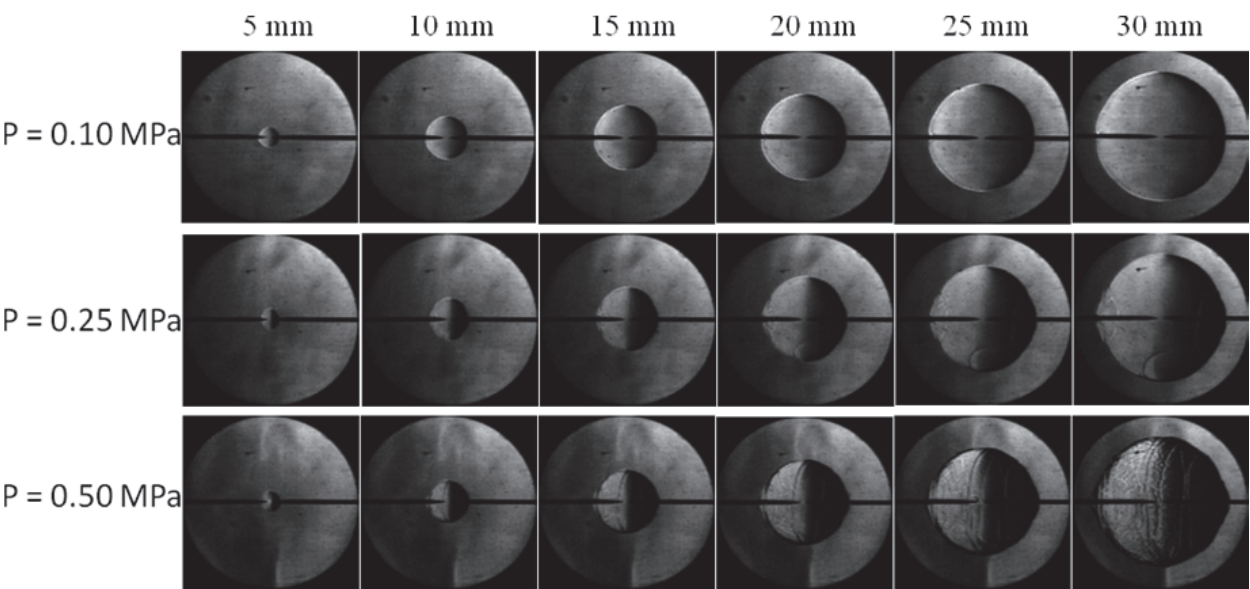


Fig. 10. Schlieren images of flames for DMF/iso-octane-air mixtures at the equivalence ratio of 1.2 and the initial temperature of 393K at three different initial pressures

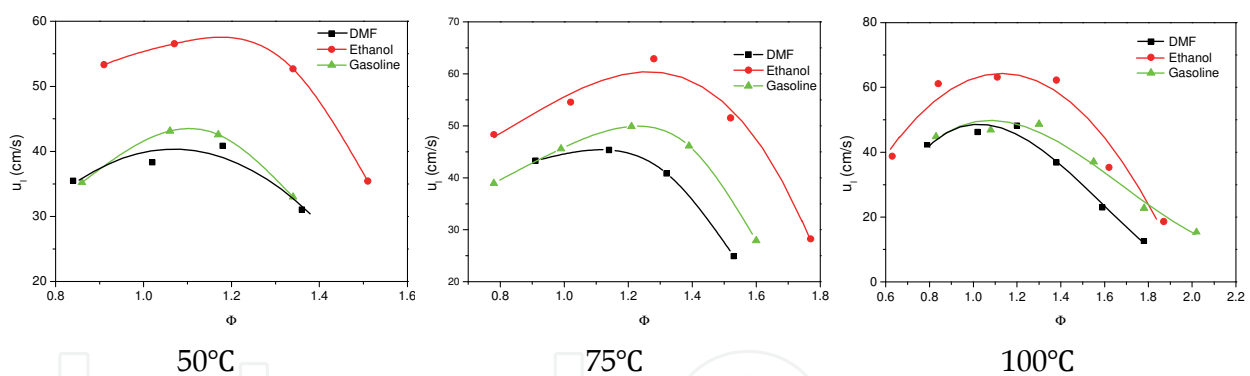


Fig. 11. Laminar burning velocities at various initial temperatures

Ethanol shows high potential in terms of its laminar burning velocity. Although the velocity decreases significantly when the equivalence ratio goes beyond 1.6, the magnitude is very high in the wide near-stoichiometry range. The difference between the laminar burning velocity of DMF and ethanol in a typical engine application region ( $\Phi=0.9-1.2$ ) is almost 30%. The curvatures of the lines within these graphs closely resemble those of other fuels under similar ambient test conditions (temperature and pressure), as documented by Heywood (Heywood 1988). He states that the peak laminar burning velocity of gasoline at 27°C is 36cm/s. In our tests, at 50°C, the peak is 44cm/s, an increase of 8cm/s. This highlights how the initial temperature affects the burning velocity. Increasing the temperature also appears to bring the peak burning velocity for the other equivalence ratios toward a maximum burning velocity. For instance, when the temperature is doubled to 100°C, the maximum remains the same, but the difference between the surrounding equivalence ratio points is

reduced. Therefore, there appears to be a maximum laminar burning velocity. This is certainly apparent for ethanol, where its maximum laminar burning velocity is approximately 62cm/s. For DMF, the maximum is less clear from the data available, but this lies somewhere in the range 41-48cm/s.

In summary, the fundamental spray characteristics and laminar flame propagation tests show how DMF has a high potential for use in spark-ignition engines. Its spray and laminar burning characteristics are very close to those of gasoline, which means it could be adopted in current spark-ignition engines without major modifications.

## 5. Engine performance and regulated emissions

Thus far, the analysis of DMF has shown promising similarities to gasoline. However, the experiments were performed in controlled environments whereas in an engine application, the local temperatures and pressures are varying cyclically. Therefore, the next step is to analyse the combustion characteristics in an engine, in order to understand the influence of the complex combination of various parameters. Within the research community, this can be achieved using single-cylinder engines.

In this section, the engine performance (for instance, optimum spark timing, fuel economy or exhaust temperature) and the regulated engine-out emissions (nitrogen oxides ( $\text{NO}_x$ ), carbon monoxide (CO) and total hydrocarbons (THC)) are discussed. Furthermore, as DMF is a new biofuel candidate, it is important to analyse the relative products of combustion. Not only is it necessary to look at solid particles but also the individual hydrocarbons. This allows us to assess the concern for the environment and to humans. Therefore, detailed analysis of the solid particles is made in the next section of this chapter.

Once more, DMF is benchmarked against gasoline and compared to ethanol. As can be expected, the three fuels have different locations of optimum spark timing (referred to as the maximum brake torque or, MBT timing) due to their differing anti-knocking properties, or octane numbers. Figure 12 shows these optimum spark timings at various engine loads for DMF, ethanol and unleaded gasoline (ULG). The indicated mean effective pressure (IMEP) is a widely used scale for engine research and represents the engine load. Unlike engine torque, which is measured from the dynamometer, the IMEP is calculated using the raw crank-angle-resolved in-cylinder pressure trace. This reflects the power directly delivered from the fuel energy to the piston, before any friction losses are considered. This method is more meaningful for engine research because the friction losses vary greatly between engines. For a naturally aspirated spark-ignition engine, the IMEP is usually around 10 bar at wide open throttle (highest load).

Figure 12 clearly shows that at low load (3.5bar IMEP) there is no difference in the MBT location between the three fuels; the spark sweeps generate a relatively flat IMEP curve around 34°bTDC. However, throughout the remaining load range, ethanol allows the most advanced spark timing due to a higher knock resistance and burning velocity. Ethanol also generates greater charge-cooling because of a higher latent heat of vaporization (840kJ/kg for ethanol, compared to 332kJ/kg and 373kJ/kg for DMF and gasoline respectively, see Table 1). This lowers the combustion temperature and reduces the end-gas auto-ignition, or knocking tendency. At the highest load, the MBT spark timing when using ethanol is 11CAD more advanced than with gasoline and 5CAD more than with DMF. Until 6.5bar IMEP, the MBT timing between DMF and ethanol is only separated by 1CAD. Despite this, the maximum IMEP when using DMF is limited by audible knock at 5.5bar IMEP and the

theoretical MBT timing cannot be achieved. Although it is believed that DMF has a higher octane number than ethanol (Yuriy Roman-Leshkov 2007), the MBT timing in the current engine testing is more retarded than that with ethanol, due to this onset of knock. The optimum spark timing for gasoline is clearly the most retarded, once again limited by knock.

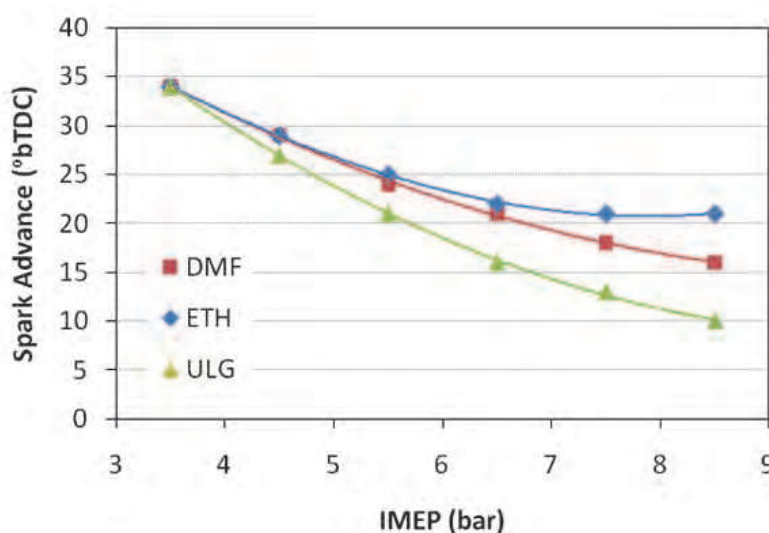


Fig. 12. Optimum Spark Timings at Various Engine Loads for DMF, Ethanol and Gasoline

When using 97 RON gasoline, a knock margin (2CAD retard) was enforced as early as 4.5bar IMEP, which restricted the ability to find the optimum MBT timing. For DMF, however, this safe margin was not enforced until 5.5bar IMEP, as previously mentioned. Although this produces an advantage in efficiency for DMF over 97 RON gasoline, in terms of knock suppression, and therefore spark advance, the anti-knock qualities of DMF are not as proficient as ethanol's due to the lower in-cylinder gas temperature associated with the latter. The studies by Gautam and Martin (Gautam 2000) have shown that the knock suppression capability of oxygen containing fuels is related to the relative oxygen content. Therefore, it is perhaps not surprising for DMF to have poorer anti-knock qualities than ethanol, as it contains less relative oxygen (see Table 1).

Figure 13(a) shows the gravimetric fuel consumption. Although there are differences between the three fuels, whereby DMF is more efficient than ethanol, Figure 13(b) is perhaps more relevant to the end user. The volumetric fuel consumption of DMF is very similar to that of gasoline, due to similar volumetric calorific values. DMF's calorific value is only 6% less than gasoline's, whereas ethanol is 33% less. Ethanol suffers from a low energy density, which would require more re-fuelling for the same volume compared to DMF.

Another fuel conversion efficiency measure is the indicated efficiency, or inversely, the gasoline equivalent indicated specific fuel consumption, or ISFCE. The indicated efficiency is defined as the ratio of the indicated power output to the lower heating value contained in the burning fuel mass. The gasoline equivalent fuel consumption is calculated using the equation shown. First, the numerator converts the fuel consumption rate into an energy rate using the lower heating value of the fuel. Then, once this is divided by the gasoline lower heating value, the fuel rate is converted to a gasoline equivalent. Clearly, the indicated efficiency and gasoline equivalent fuel consumption are inversely proportional. Introducing



these two parameters allows a direct comparison of the energy conversion efficiency of the fuel between DMF, gasoline and ethanol. The ISFCE normalizes the lower heating value relative to gasoline and so presents a similar trend and offset as found with the indicated efficiency.

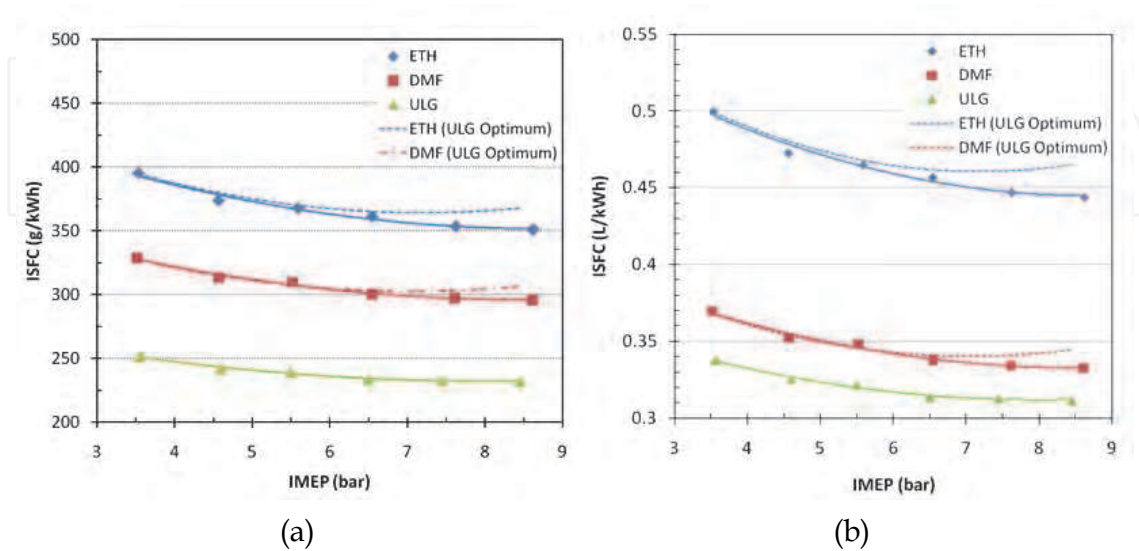


Fig. 13. (a) Gravimetric and (b) Volumetric Indicated Specific Fuel Consumption

$$ISCE_x = \frac{ISFC_x \times LHV_x}{LHV_{ULG}} \tag{8}$$

Figure 14 highlights the relationship between the indicated efficiency and the ISFCE between the three fuels. Under gasoline MBT timing, as shown by the dashed and dashed-dot lines for ethanol and DMF respectively, the three fuels reach an efficiency peak between 7 and 7.5bar IMEP. Although the curvature is similar, the offset is different. Using advanced modeling software, the authors calculated that DMF burns at the highest combustion temperature, which should lead to a higher thermodynamic efficiency. However, this effect is compensated by the higher heat exchange loss. This is also reflected in the ISFCE. Therefore, this preliminary work suggests that DMF is less efficient than ethanol in transferring the fuel energy into useful engine work when using the fuel-specific MBT timing. Nevertheless, both fuels are competitive to gasoline, especially at high engine loads.

The exhaust gas temperature is another important parameter because it influences the catalyst converter and turbocharger performance (if equipped). Figure 15 shows the exhaust gas temperature 55mm downstream of the cylinder head for the various loads and spark timings between the three fuels. Ethanol combustion clearly results in the lowest exhaust temperature. The reason for this is twofold. Firstly, ethanol has a relatively high latent heat of evaporation, which absorbs more heat in the compression stage. Secondly, the MBT timing for ethanol is much more advanced than for DMF and gasoline, which leads to lower in-cylinder temperatures when the exhaust valves open as the combustion process completes earlier. This also means that more energy is extracted from the burned gas to deliver the useful work, which can explain the higher efficiency seen in Figure 14. When using DMF, the exhaust temperature is approximately 30°C lower than with gasoline at the



highest load when using the fuel-specific MBT timing. However, for ethanol, this drop is more than double that seen with DMF (approximately 65°C). As previously mentioned, ethanol has more advanced MBT timing, which advances the combustion and causes a lower exhaust temperature. This effect can be seen when comparing the gasoline specific MBT timing with the fuel-specific MBT timing. When using DMF, for instance, at gasoline MBT timing, the temperature difference between DMF and gasoline is negligible (shown by the dotted line). However, when the spark timing is optimized, the exhaust temperature when using DMF drops significantly. At these temperatures the exhaust gas temperatures are suitable for the efficient performance of three-way catalysts. However, when using a turbocharger, which is likely to become more prominent with engine downsizing, it is more useful to have higher exhaust gas temperatures, so that there is more potential to extract useful energy.

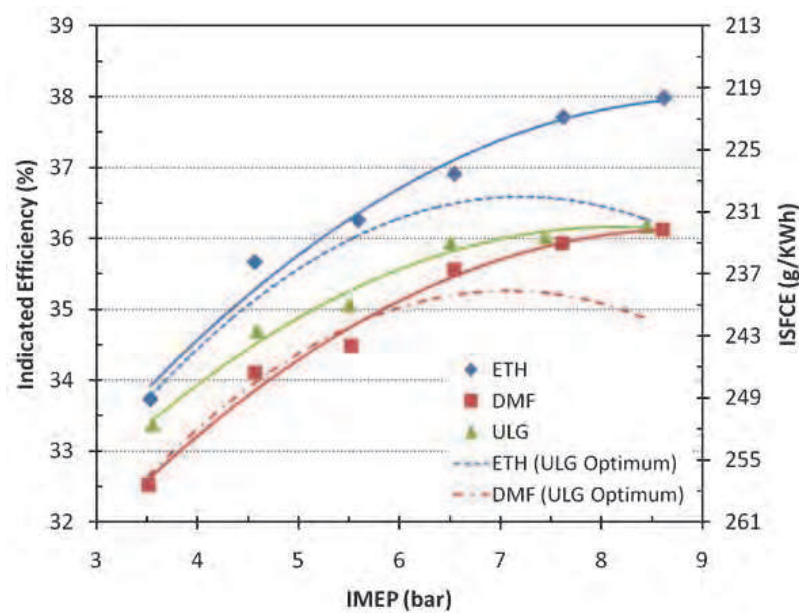


Fig. 14. Indicated Efficiency/Gasoline Equivalent Indicated Specific Fuel Consumption

In spark-ignition engines, the necessity to throttle the intake air causes a restriction to the flow, which leads to pumping losses (not seen in diesel engines). This pumping loss is one of the main reasons why spark-ignition engines have lower efficiency than compression-ignition engines. The volumetric efficiency, which can be thought of as opposite to the pumping loss, is defined as the ratio between the actual intake air mass and the maximum theoretical intake air mass without any losses. The comparison of the pumping losses between DMF and ethanol is shown in Figure 16. This loss directly affects the fuel economy and the differences between the two fuels can be better explained by their physicochemical properties. As shown in Table 1, ethanol contains more oxygen atoms, by weight, which results in a lower stoichiometric air-fuel ratio, or AFR. This reduces the throttle angle demand and as a result increases the net pumping loss and fuel consumption. On initial inspection, this behavior explains the trend of the volumetric efficiency compared to DMF and gasoline (Figure 16). At lower loads (<6bar IMEP), there is little difference in the volumetric efficiency between the oxygen content fuels. However, at higher loads ( $\geq 6$ bar IMEP), the separation is more evident, which demonstrates the effect of ethanol's low stoichiometric AFR. For gasoline, whose stoichiometric AFR is much higher (14.5), the

volumetric efficiency is superior because more air is required to compensate for no oxygen in the fuel. However, with closer inspection of the pumping losses, or pumping mean effective pressure (PMEP) below 6bar IMEP, ethanol overcomes the higher throttling requirement. This is largely due to the higher charge-cooling effect of ethanol. At 3.5bar IMEP, the pumping loss, when fuelled with DMF at gasoline MBT timing is 48.9kPa, whereas for ethanol the loss is 47.9kPa. This represents an advantage to ethanol of 1kPa. At 8.5bar IMEP, this advantage shifts in DMF's favor by 2.1kPa (15.7kPa for DMF and 17.8kPa for ethanol). This reduction in pumping loss for ethanol at low load could be attributed to its high heat of vaporization. This effect on volumetric efficiency in a direct-injection spark-ignition engine is well documented by other researchers (Heywood 1988; Stone 1999). Therefore, the relatively high charge-cooling effect created when the ethanol fuel is injected and then evaporated, counteracts the pumping loss due to throttling. As the fuel is injected, the in-cylinder temperature reduces as the fuel vaporizes. This increases the density of the intake air, which allows more air to be consumed. Following the cross-over with DMF at 6bar IMEP, the charge-cooling advantage is then superseded by the much higher throttling losses at higher load.

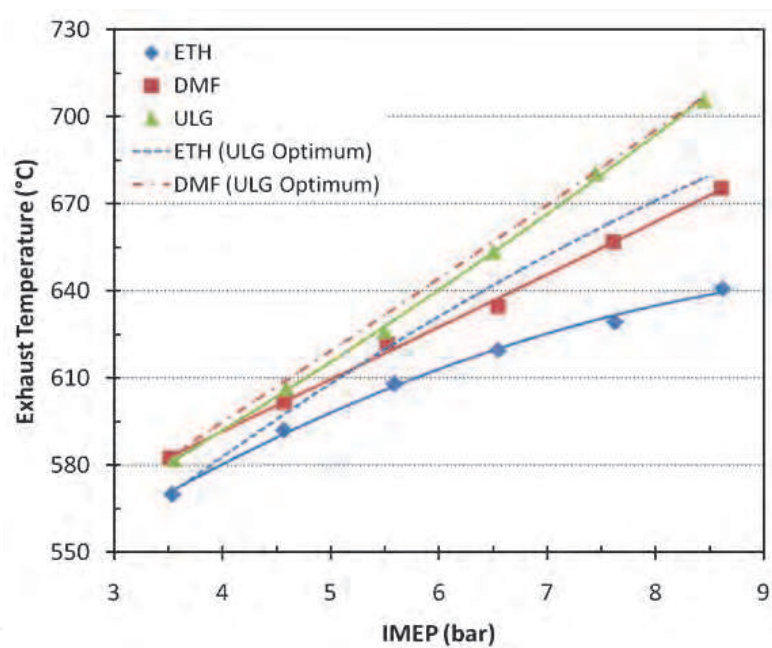


Fig. 15. Exhaust Gas Temperatures

The maximum in-cylinder pressures  $P_{max}$ , or peak pressure, for the three fuels are shown in Figure 17. At low load, the difference between these three fuels is marginal, but as the load increases, the peak pressures of ethanol and DMF are significantly higher than that with gasoline. At loads higher than 6.5bar IMEP, the peak pressure when using ethanol exceeds that when using DMF. At 8.5bar IMEP, the peak pressure with ethanol is 7bar higher than with DMF and almost 20bar higher than with gasoline. In Figure 17, the peak pressures of ethanol and DMF when using the MBT timing for gasoline are shown with dashed and dashed dot lines respectively. The difference between the three fuels is negligible and is explained by the different combustion speeds. Although the laminar burning velocity data is available from previous research, it is the turbulent burning velocity which dominates the combustion speed. Without going into depth on the fundamentals of turbulent combustion

theory, the combustion speed is normally determined by the in-cylinder pressure trace and is defined as the period in crank angle degrees or, CAD, between 10 and 90% of the total energy released, or mass fraction burned (MFB). This combustion duration data for the three fuels is shown in Figure 18.

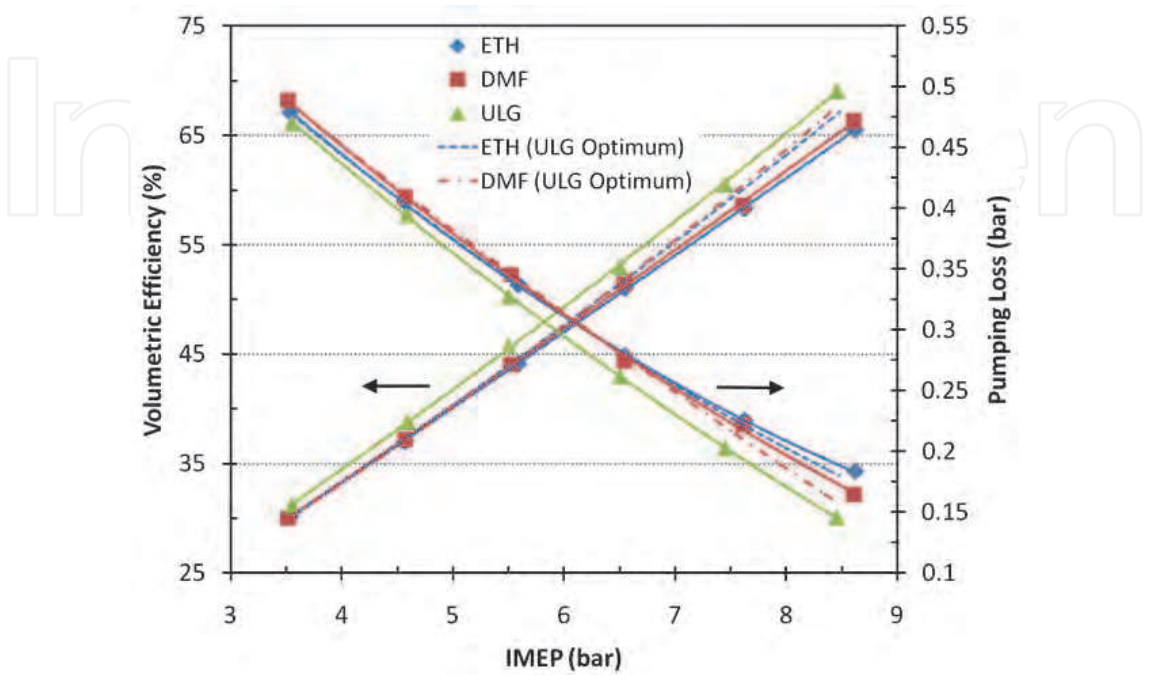


Fig. 16. Volumetric Efficiency and Pumping Losses

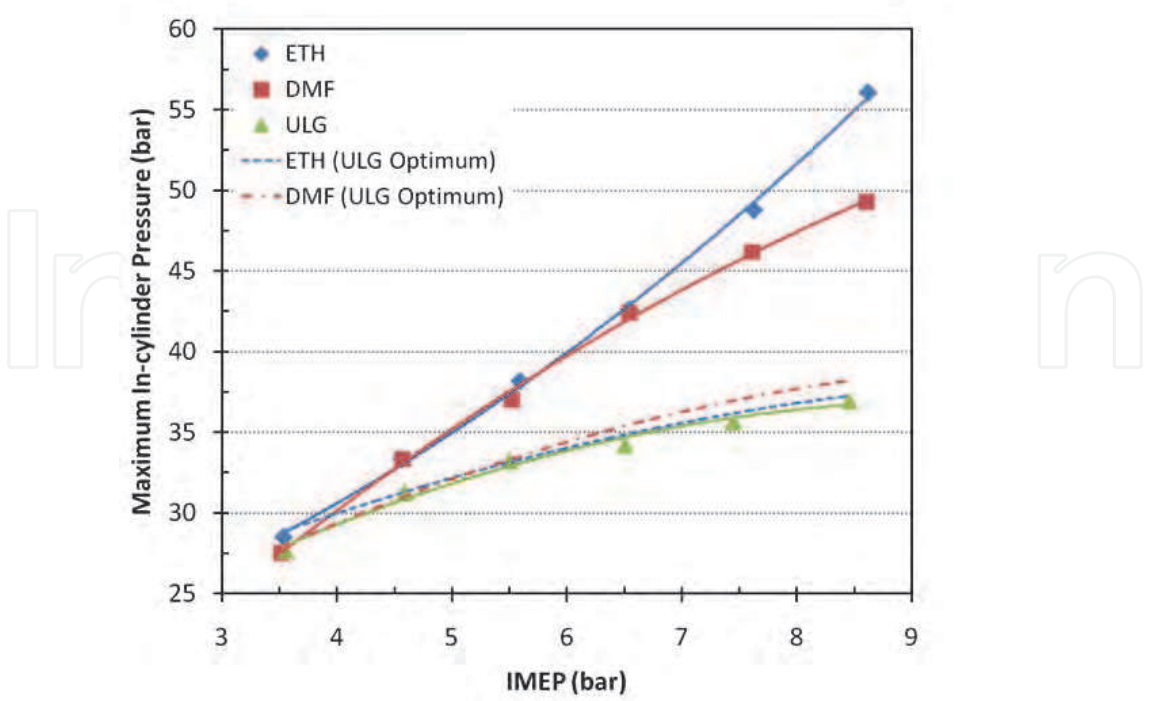


Fig. 17. Maximum In-cylinder Pressure

Evidently, when using the fuel-specific MBT timing, the combustion speeds for both DMF and ethanol are higher than with gasoline. At 8.5bar IMEP, the combustion of the oxygen content fuels ends approximately 4CAD before gasoline. However, between the two oxygen content fuels, the combustion duration when using DMF is marginally lower, than for ethanol. Apart from the low and high loads (3.5bar and 8.5bar IMEP respectively), the combustion duration of DMF is at least 0.35CAD lower, than with ethanol. At fixed gasoline MBT timing, it is again DMF that burns the fastest (apart from 3.5bar IMEP). At 8.5bar IMEP, DMF burns 1CAD quicker than ethanol and 1.3CAD quicker than gasoline. That explains why at this point, DMF has slightly higher peak in-cylinder pressures than ethanol.

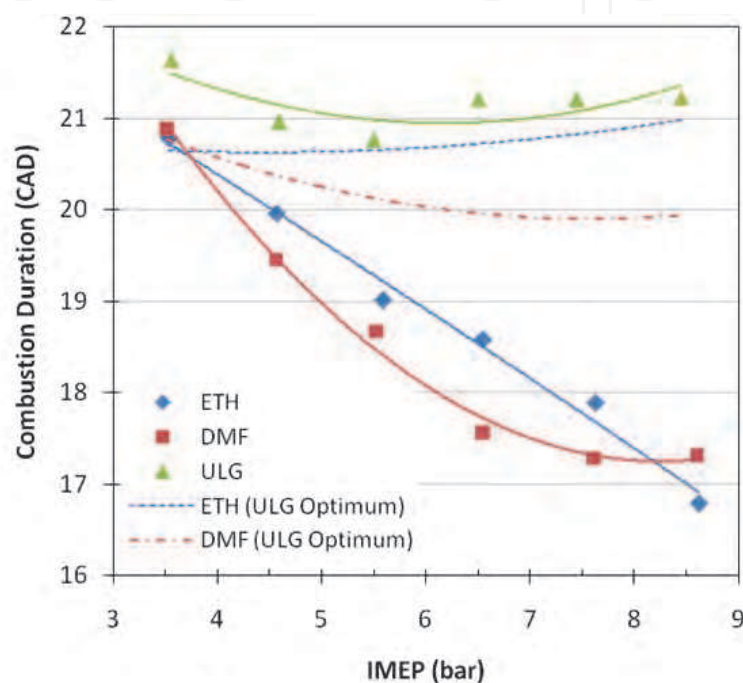


Fig. 18. Combustion Duration (10-90% MFB)

With further analysis of the combustion event, we can study the combustion duration either side of the 50% MFB point, or CA50 when using the gasoline MBT timing. At 8.5bar IMEP, DMF combustion is shown to be consistently quicker than both ethanol and gasoline. This is shown in Figure 19. For all three fuels, the duration before CA50 (10-50% MFB), is slightly higher than that afterwards (50-90% MFB). For DMF, the 10-50% MFB duration is 10.75CAD compared to 9.2CAD for the 50-90% MFB duration, which represents a difference between ethanol of 0.12CAD and 0.83CAD respectively. For DMF and gasoline, the reduction in duration after the CA50 location is 15% and 12% respectively. However, for ethanol this reduction is limited to 8%. Although at this load, ethanol burns more quickly than gasoline before CA50, afterwards gasoline is superior.

These results highlight the advantage of the burning speed of DMF combustion compared to that when using ethanol despite having a lower measured laminar flame speed which was introduced previously. Overall, however, under these test conditions, both oxygen content fuels burn more quickly than gasoline.

The engine-out emissions are compared between the three fuels at the various loads and spark-timing conditions. Firstly, the regulated emissions, which include nitrous oxides



(NO<sub>x</sub>), unburned total hydrocarbons (THC), and carbon monoxide (CO) emissions are evaluated. This is followed by an analysis of the carbon dioxide (CO<sub>2</sub>) emissions.

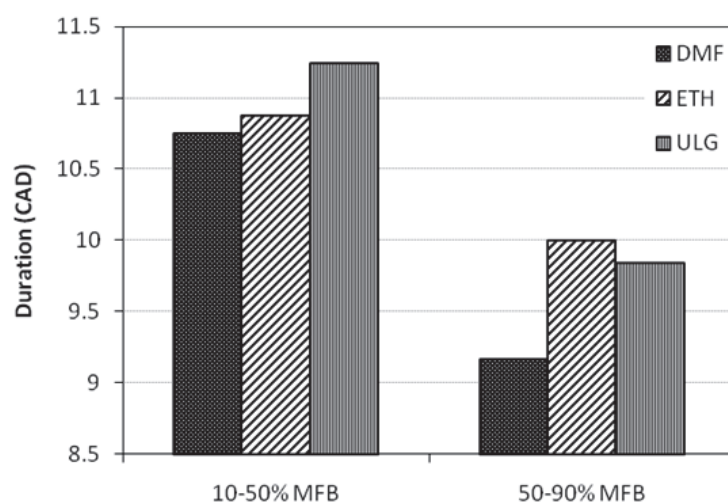


Fig. 19. Combustion Durations either side of CA50 (8.5bar IMEP, Gasoline Optimum Spark Timing)

NO<sub>x</sub> is one of most concerning engine-out emissions. It is 20 times more toxic than CO and is the main component to cause photochemical smog. The formation of NO<sub>x</sub> mainly occurs when the combustion temperature exceeds 1800K and the mixture is locally rich of oxygen. The indicated specific NO<sub>x</sub> (isNO<sub>x</sub>) emissions are illustrated in Figure 20. The indicated specific emissions shows the mass of emissions gas from the engine with each unit of power produced and has the units of g/kWh. It is clear that the isNO<sub>x</sub> production is load dependant and generally increases with load. When using the same spark timing, ethanol produces much lower isNO<sub>x</sub> emissions compared to gasoline. This is because ethanol burns at a relatively higher rate and with a lower combustion temperature. Although DMF appears to have a marginally quicker burning rate than ethanol, the isNO<sub>x</sub> emissions are more similar to gasoline because the combustion temperatures are much higher. For fuel-specific optimum ignition timing, the production of isNO<sub>x</sub> emissions increases. For ethanol, this increase with load is much larger than for DMF. Above 7.5bar IMEP, the emissions are now comparable with gasoline. Optimized MBT timing for ethanol is 11CAD more advanced than the gasoline optimum spark timing, which rapidly increases the in-cylinder pressures. The peak combustion pressures for DMF are similar to ethanol but the temperatures are somewhat higher due to the lower charge-cooling effect. The relative isNO<sub>x</sub> emissions can also be attributed to the H/C ratio. Ethanol, which produces the lowest isNO<sub>x</sub> emissions, is the highest H/C ratio fuel, whereas DMF produces the highest isNO<sub>x</sub> emissions and has the lowest H/C ratio. Therefore, the isNO<sub>x</sub> emissions have an inverse relationship to the H/C ratio of the fuel.

The indicated specific total hydrocarbon emissions (isTHC) are much lower for ethanol at all conditions, than for DMF and gasoline, as suggested in Figure 21. Ethanol's oxygen content is much higher than DMF, which, together with it's high combustion efficiency, aids the oxidation of unburned hydrocarbons as oxygen is more readily available. As the load increases from 3.5 to 8.5bar IMEP, the isHC emissions decrease by approximately 30% for all fuels. This is due to increased combustion temperatures and thus combustion efficiency. The



HC and CO emissions reduce due to greater oxidation of the hydrogen and carbon molecules. However, the level of isTHC emissions produced from DMF combustion is between that with gasoline and ethanol.

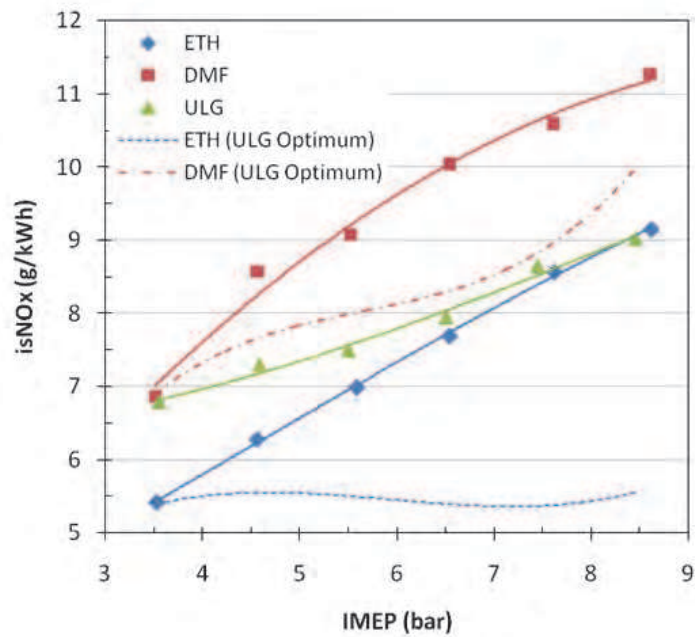


Fig. 20. Indicated Specific NO<sub>x</sub> Emissions

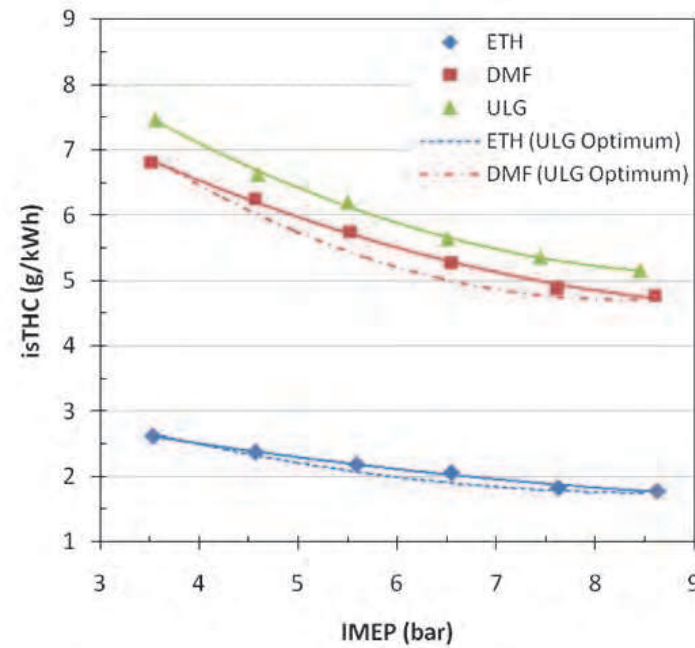


Fig. 21. Indicated Specific Total Hydrocarbon Emissions

The indicated specific carbon monoxide emissions (isCO) comparison between the three fuels is made in Figure 22. Similarly to the isTHC emissions, the isCO emissions generally decrease as load increases. This trend is similar to the inverse of indicated efficiency, where the lowest isCO emissions arise at the highest efficiency. Between the two oxygen content fuels, ethanol consistently produces the lowest isCO emissions for all test conditions. This is due to a higher combustion efficiency and oxygen content. Under gasoline optimum spark timing, the difference increases with load. At 3.5bar IMEP, ethanol is 1g/kWh lower, whereas at 8.5bar IMEP this difference increases to 3g/kWh. Under fuel-specific optimum ignition timing the largest difference is seen at medium loads. For gasoline, the relationship with respect to load is less predictable. The peak at 4.5bar IMEP could be explained by the relatively lower combustion efficiency at this point. At this load, the mixture may be inhomogeneous, resulting in localized pockets of fuel-rich mixture and more incomplete combustion. However, the remaining isCO emissions fluctuate within a similar range as the two biofuels, which all decrease to a minimum around 7.5bar IMEP.

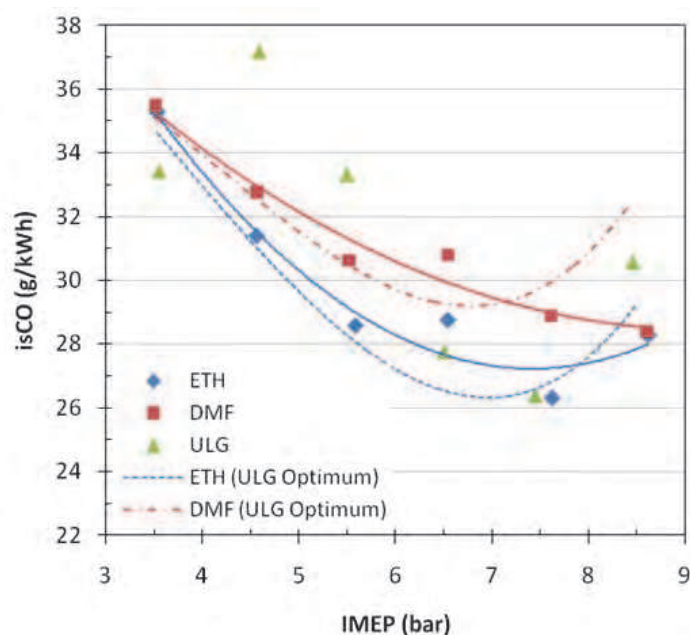


Fig. 22. Indicated Specific Carbon Monoxide Emissions

Although carbon dioxide ( $\text{CO}_2$ ) is a non-toxic gas, which is not classified as a pollutant engine emission, it is one of the substances responsible for global warming through the greenhouse effect. Therefore, a consideration of the indicated specific  $\text{CO}_2$  (is $\text{CO}_2$ ) production is made between the three fuels. This is shown in Figure 23. Here, the is $\text{CO}_2$  emissions decrease with increasing load and advancing ignition timing towards the optimum spark timing. The is $\text{CO}_2$  emissions are an indication of the completeness of combustion. Therefore, as the load is increased, the combustion is more complete, which is shown by the increase in combustion efficiency. When using gasoline optimum spark timing, DMF and ethanol combustion produces a peak in efficiency between 6 and 7bar IMEP and a minimum in is $\text{CO}_2$ . Although both biofuels produce higher engine-out is $\text{CO}_2$  emissions than gasoline, they both have the added benefit of consuming the  $\text{CO}_2$  in the atmosphere during their raw production. Therefore, it is fairer to compare the relative lifecycle  $\text{CO}_2$  emissions.

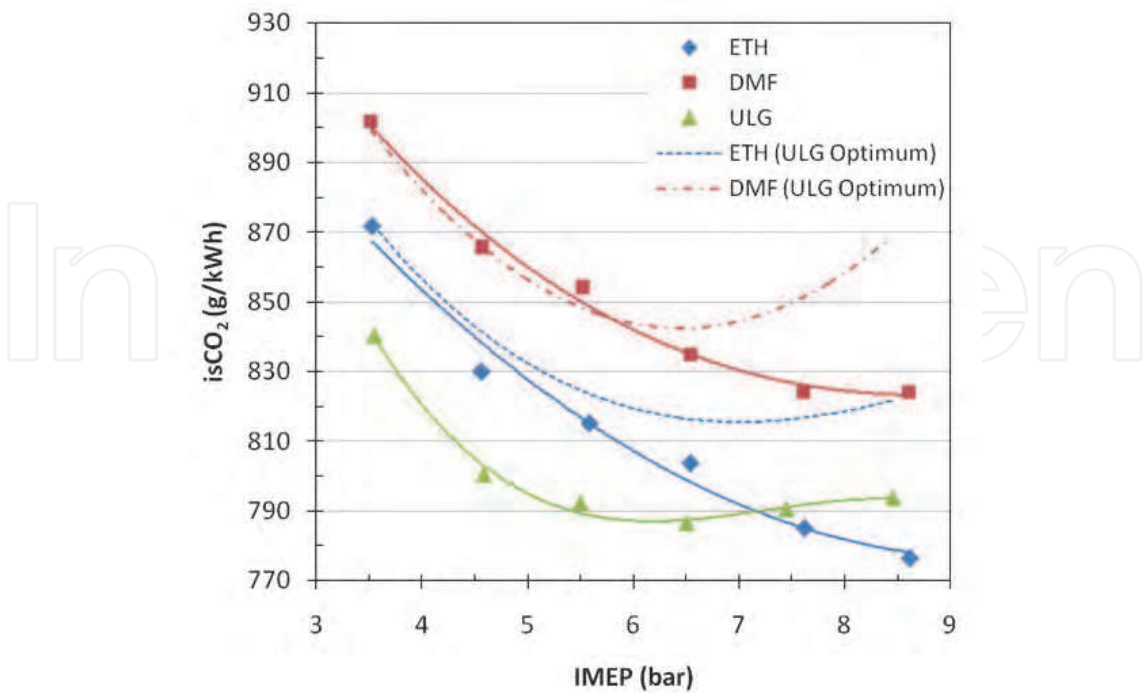


Fig. 23. Indicated Specific Carbon Dioxide Emissions

The engine tests further highlight the competition DMF creates with ethanol in replacing gasoline as a spark-ignition fuel. Due to ethanol’s ability to suppress knock, the engine could be run at more advanced spark timing conditions allowing the optimum or MBT timing to be used. The optimized timing for DMF and gasoline, however, was limited by engine knock, and so was retarded. Despite this, DMF was more resistant to knock than gasoline, which suggests that DMF’s octane rating is between that of ethanol (approximately 110 RON) and 97 RON gasoline. Despite this, the speed of combustion when fuelled with DMF was faster than that with ethanol. In fact, both DMF and ethanol have lower initial and total combustion durations than gasoline. These lower combustion durations were further reduced when the ignition timing was optimized, highlighting the rapid combustion of these oxygen content fuels. Additionally, the volumetric fuel consumption rate of DMF is similar to that of gasoline. This suggests that a consumer using DMF as a substitute for gasoline, would benefit from a similar range with the same volume of fuel. Although the indicated efficiency of DMF is lower than gasoline, there is potentially more extractable energy in the exhaust gas. Finally, in terms of engine-out emissions, the results for DMF were similar to that with gasoline. The only penalty was seen in the way of NO<sub>x</sub> emissions, which would be reduced through the catalytic converter. These NO<sub>x</sub> levels were also higher than that for ethanol, mainly due to the higher combustion temperatures. Ethanol’s higher latent heat of vaporization offers better charge-cooling. However, this does introduce cold-start issues which would not be experienced when using DMF.

In the next section, an overview of the unregulated emissions is made. This focuses on the solid particles which are produced through DMF combustion. This is then followed by an investigation of a novel approach for the improved use of biofuels in spark-ignition engines through the dual-injection fuelling system.

## 6. Unregulated emissions

Currently, the particulate matter (PM) emissions do not form part of the emissions legislations for gasoline spark-ignition engines in Europe or the US. However, control of these emissions is expected to commence in European and US regulation in 2014. This will require, not only the monitoring of particulate mass, but also the particulate number for all light-duty vehicles. Therefore, an understanding of these emissions will become much more important and it is necessary to understand the implication of the PM emissions when using biofuels. In this section, the PM emissions between the three fuels is studied at low and high load.

The PM size distributions for the three fuels at 3.5bar IMEP using gasoline MBT timing (34°bTDC), are shown in Figure 24 (a). Typically, the PM size distribution consists of two modes: the accumulation and nucleation modes. The former consists of solid carbonaceous species usually greater than 50nm in diameter, whereas the latter consists of liquid particles usually less than 50nm in diameter. The separation between the nucleation and accumulation modes is shown clearly by the peak in the size distributions around 50nm in Figure 24 (a). At this low load, the size distribution shows marginally more accumulation mode particles than nucleation ones. For gasoline, 62.1% of the total particles are accumulation mode particles, whereas for DMF and ethanol, this rises to 64.4 and 67.1%, respectively. The difference between DMF and ethanol is 21,805particles/cm<sup>3</sup>. This might be caused by DMF's lower viscosity and surface tension, which leads to smaller injected fuel particles. Also, the in-cylinder temperature when using ethanol has been seen to be much lower than that for DMF. This is caused by the greater charge-cooling effect when using ethanol, which counteracts the benefit that the higher oxygen content would have in helping to lower the PM emissions.

The PM size distributions are also compared at 8.5bar IMEP using gasoline MBT timing (10°bTDC). This is shown in Figure 24 (b). Evidently, the effect of load has a significant impact on the PM emissions. The separation between the nucleation and accumulation modes is shown clearly by the inflection in the size distributions around 50nm in Figure 24 (b). Here, the nucleation mode particles dominate the particle size distribution for each fuel, with peaks between 25-30nm. For ethanol and DMF, the accumulation mode now only represents 2.1 and 1.7% of the total particle concentrations, respectively. However, for gasoline, the proportion of accumulation mode particles is much higher (18.3%). In absolute terms, gasoline combustion also produces more accumulation mode particles than when fuelled with the biofuels; both biofuels produce less than 4,000particles/cm<sup>3</sup>, whereas gasoline produces almost 21,000particles/cm<sup>3</sup>. This is likely to be caused by the higher droplet velocity of gasoline and relatively high mean droplet diameter, found in previous studies. This could increase the impingement on the piston surface, which would explain the relatively lower combustion efficiency. At this load, the biofuels also burn at higher pressures and temperatures, which helps to promote pyrolysis and further reduce the solid carbonaceous emissions. The opposite is true, however, for gasoline when considering the nucleation mode concentration at 8.5bar IMEP. Now, gasoline combustion produces a similar amount of particles to that of ethanol, and DMF is the worst offender; almost 122,000particles/cm<sup>3</sup>, or 30% more particles are produced when using DMF. This relative increase in nucleation mode particles for DMF was seen in previous experiments by the authors and is likely to be caused by the incomplete combustion of the ring structure of DMF, which are known to be soot precursors.

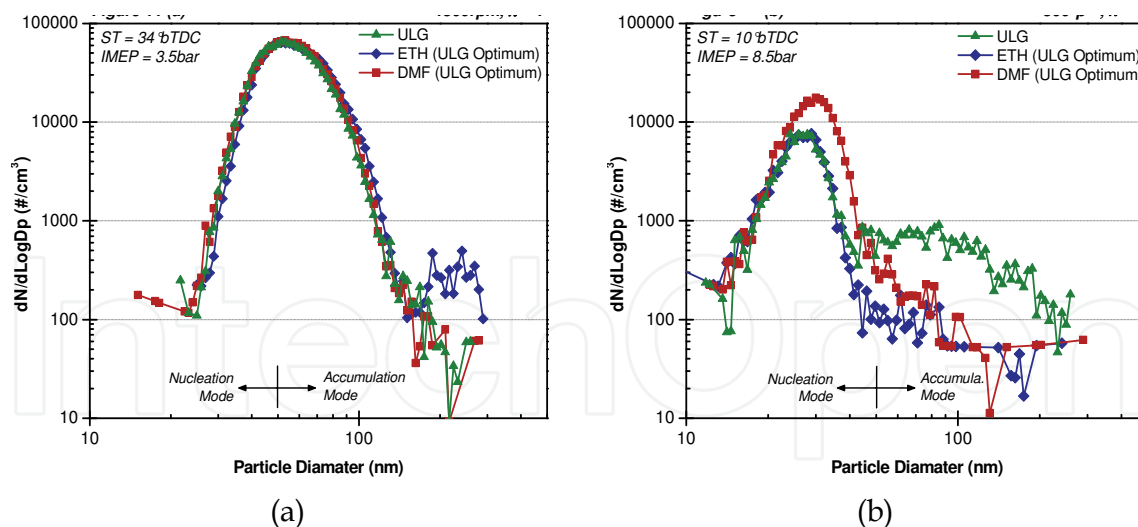


Fig. 24. (a) PM Size Distributions at 3.5bar and (b) 8.5bar IMEP using Gasoline MBT/KL-MBT Timing

In summary, the PM emissions for DMF have been shown to be comparable to that of gasoline at low load. At a higher concentration of load, DMF produces high nucleation mode particles compared to gasoline but a lower concentration of accumulation mode particles. Compared to ethanol, DMF shows similar sized accumulation mode particles at high load, which helps to reduce the average particle size.

The PM emissions work is ongoing and further results are likely to follow in publications by the authors. Furthermore, individual hydrocarbon speciation will show more details of the toxic compounds which are emitted from DMF, ethanol and gasoline and help to better understand the potential effect on the environment and to human health.

## 7. Dual-Injection - a potential method to utilise biofuels

There are many different approaches to partially substitute biofuels for gasoline. The simplest method is to run the engine on a blend of biofuel and gasoline which is supplied at the pump and so externally mixed. This, however, requires a fixed blend ratio to allow the engine to always run in the optimized condition. Alternatively, engines can have flex-fuel capability, with an ability to be smart enough to recognise different blend ratios at any moment and adapt the control strategy to reflect the change in fuel supply. This method is commonly used across Brazil for any blend of ethanol and gasoline. However, another approach is the so-called dual-fuel system. This method, which is referred to as dual-injection in this chapter, also increases system complexity similarly to a flex-fuel vehicle. However, dual-injection offers improved flexibility and control of the instantaneous blend ratio.

In the dual-injection tests, gasoline, is supplied as the main fuel and is delivered through a port-fuel injection (PFI) system. This is then gradually substituted by the supplementary fuel (DMF, ethanol and gasoline) using the direct-injection (DI) system in order to reach the required AFR. Both injectors were calibrated to enable the precise control of the blend ratio at any point. For all stable conditions the engine was run at the stoichiometric AFR and constant preset throttle positions (for simplicity). As fractions of PFI gasoline were replaced by the DI fuel, improved volumetric efficiency and load outputs were expected as the throttle was kept constant. Of course, much more calibration work is required to fully realise



this method. However, the use for this approach in real production engines is very promising.

The results in this section are shown using stacked graphs to reflect the three initial engine load conditions (represented by initial manifold air pressure,  $MAP_i$ ) using PFI gasoline. For each normalized graph, the vertical axis shows the relative change in each key parameter from the 100% PFI condition. The horizontal axis shows the reduction in the PFI mass fraction, also from the 100% PFI condition, which has been compensated for using DI fuelling to maintain stoichiometry. Error bars have been used to highlight the test repeatability for the three repeats.

Figure 25 shows the relationship between the normalized volumetric air flow rates with varying PFI mass fraction for the three fuels at the three different initial engine loads. It is clear that the volumetric air flow rate increases with decreasing PFI mass fraction regardless of the  $MAP_i$  and the DI fuel used. This is mainly because of the improved charge-cooling effect and lower PFI partial pressure. For gasoline, the maximum increase in volumetric air flow rate at the  $MAP_i$  of 0.065MPa is 1.1%. The vaporization of the gasoline causes the intake air to cool, which increases its density and thus allows more air to flow into the cylinder. Meanwhile, the partial pressure of the PFI fuel decreases with decreasing PFI mass fraction and further contributes to the improvement in volumetric air flow rate. The increase in volumetric air flow rate for ethanol in DI is much higher than that seen with gasoline and DMF, regardless of the  $MAP_i$ . This is caused by two reasons. Firstly, ethanol has a much higher latent heat of vaporization, which results in more charge-cooling. Secondly, ethanol has a lower stoichiometric AFR. Therefore, in order to maintain stoichiometry, more ethanol is required, which amplifies the aforementioned reduced partial pressure effect. For DMF, the latent heat of vaporization is marginally lower than that for gasoline. Although this would help with engine cold starts, it produces less charge-cooling when the engine is warm. However, DMF has a lower stoichiometric AFR compared to gasoline, which requires more fuel at the same  $MAP_i$ . Therefore, the combined effects of the latent heat of vaporization and the stoichiometric AFR make the volumetric air flow rate of DMF fuelling comparative to that of gasoline. Nevertheless, the anticipated improvement with volumetric air flow rate is seen consistently throughout the dual-injection strategy and so offers benefits over the 100% PFI case.

The increase in volumetric air flow rate requires more fuel flow to maintain stoichiometry. Therefore, it is reasonable to expect a higher engine load output (IMEP) as the PFI fraction is reduced. This behaviour is shown in Figure 26. Firstly, it is useful to observe this effect when fuelled with gasoline in PFI and DI. Even at low  $MAP_i$ , the increase in load was 1%, where at high  $MAP_i$  this increases to 5%. Further improvements were obtained using the two biofuels. At high  $MAP_i$ , 100% ethanol and DMF in DI produced improvements of 12% and 7% respectively, with near-linear improvements as the PFI fraction was reduced. Even at low  $MAP_i$ , the increases of 6% and 2% are notable, for ethanol and DMF, respectively. For all three fuels, the improvement in engine load is due to the improved volumetric efficiency, as previously highlighted. This effect was enhanced when using ethanol and DMF largely due to the lower stoichiometric air fuel ratios compared to gasoline. This means that more fuel is required to maintain stoichiometry. Despite the slightly lower volumetric energy density of DMF, due to the lower stoichiometric AFR, more fuel energy is supplied to the cylinder when using DMF than with gasoline. The effect of stoichiometric AFR on the volumetric efficiency is further enhanced when using ethanol, due to the higher latent heat of evaporation. This leads to a strong charge-cooling effect and allows even more fuel to be delivered as the density of the intake air increases. The combination of these two factors allows the dual-injection strategy to benefit from the increased energy output.

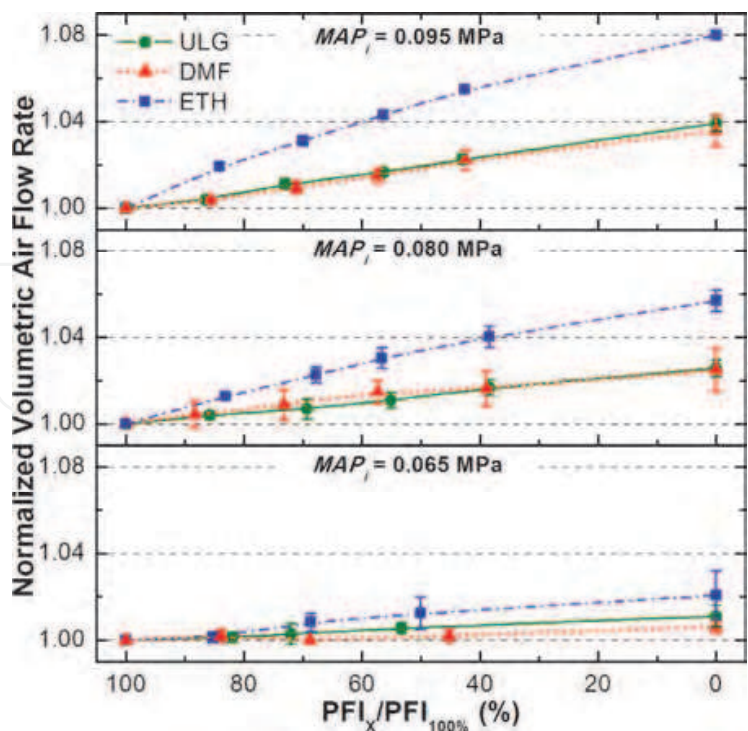


Fig. 25. Normalized Volumetric Air Flow Rate to 100% PFI condition with reduced mass fractions of PFI fuelling using Gasoline, DMF and Ethanol at three different MAP<sub>i</sub>

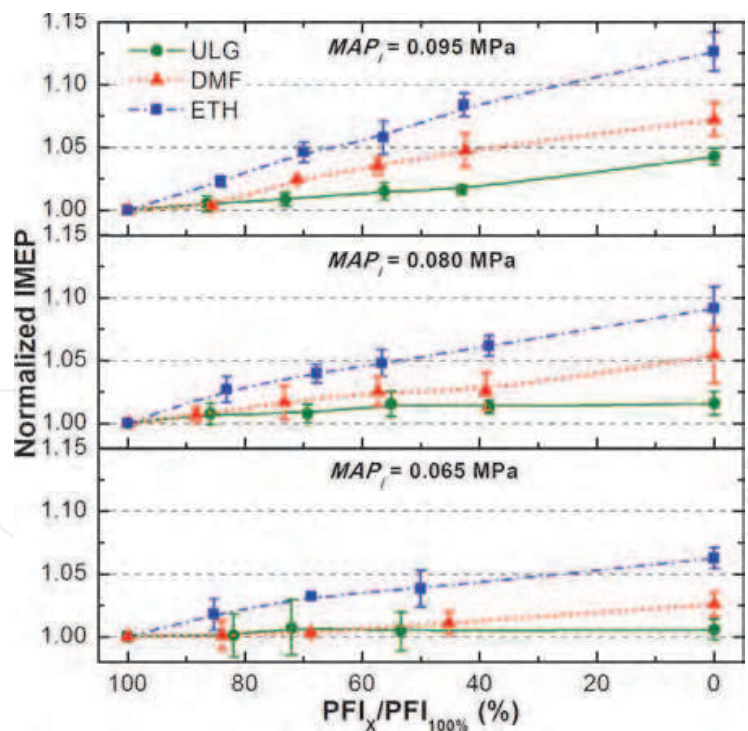


Fig. 26. Normalized IMEP to 100% PFI condition with reduced mass fractions of PFI fuelling using Gasoline, DMF and Ethanol

The indicated thermal efficiency, which is shown in Figure 27, presents varying trends between each DI fuel used. It is ethanol that shows the greatest improvements to efficiency compared to the 100% PFI case. This is apparent from as low as 85% PFI mass fraction. This

highlights the high combustion and fuel conversion efficiency of ethanol compared to gasoline and DMF in DI. In Section 5, ethanol was shown to produce 1.2g/kWh lower gasoline equivalent fuel consumption compared to gasoline when using fixed gasoline timing at high load. This gap was increased to 11.2g/kWh when the timing was optimised. This suggests that further improvements to the indicated efficiency can be made through parameter optimization. DMF, on the other hand, produces less indicated efficiency than the other fuels and even 100% PFI in most instances. For most of the test conditions the gap between DMF and gasoline increases with higher mass fractions of DMF in DI. The lower efficiency of DMF, which has been discussed in Section 5 when using pure fuels, seems to have the same effect when using blended fuels. However, both injection timing (which affects mixture generation) and ignition timing were not optimized and the improvement of engine economy is expected when fuelled with DMF with more careful calibration work.

The additional blend control parameter is one of the attractions of the dual-injection system. The engine management system (EMS) would have the flexibility to choose between different fuels and blend ratios at any moment in the engine speed and load map. For instance, when fuel economy becomes a priority, the EMS can decide to run with the lowest fuel consumption strategy. Alternatively, when maximum engine power is the main requirement, the EMS will choose the highest power output strategy. Furthermore, any issues which arise when using the 100% fuel can be overcome. For instance, ethanol is known to suffer from cold starts due to the lower heat of vaporisation. Therefore, on engine warm-up, 100% PFI gasoline could be used until the engine is warm at which point ethanol can begin to be utilised. The availability and cost of the biofuels also play an important role when choosing the current operating strategy in order to optimise the system.

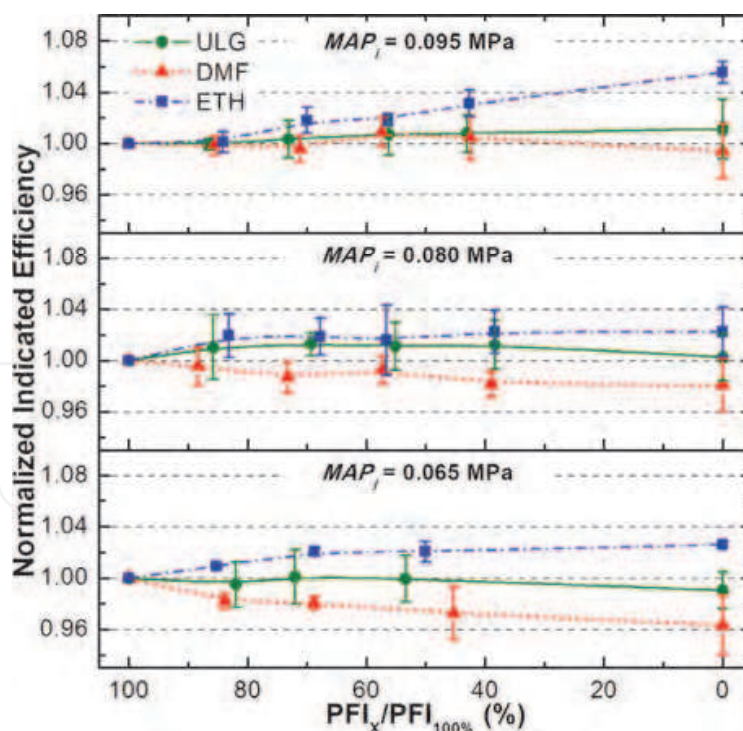


Fig. 27. Normalized Indicated Efficiency (IE) to 100% PFI condition with reduced mass fractions of PFI using Gasoline, DMF and Ethanol

The engine-out emissions produced during the dual-injection strategy are discussed below. Previously, in depth discussions were made concerning regulated, unregulated, gaseous



and particulate emissions. Therefore, this section only concerns itself with three major emissions: THC,  $\text{NO}_x$  and  $\text{CO}_2$ .

Figure 28 illustrates the indicated specific hydrocarbon emissions using the different fuels at the different  $\text{MAP}_i$ . When using gasoline in DI, the isHC emissions marginally increase at low  $\text{MAP}_i$  as the PFI mass fraction is decreased. However, as the load is increased, the effect of gasoline in DI reduces the isHC emissions. Many researchers have proved the benefit of HC reduction for direct-injection at high load (Zhao 1999), because unlike the fuel evaporation process in the intake manifold for port fuel injection, the higher injection pressure for DI offers an improvement of liquid fuel atomization and a reduction of wall wetting. When using increased fractions of ethanol or DMF in DI, the increase of the direct-injection mass fraction reduces the isHC emissions, regardless of the  $\text{MAP}_i$ . Both DMF and ethanol contain an oxygen atom in their molecular structures, which helps to reduce the HC emissions, as oxygen is more readily available. The higher relative increase in IMEP (Figure 26), together with the more readily available oxygen atoms, improves the oxidation rate of the unburned hydrocarbons.

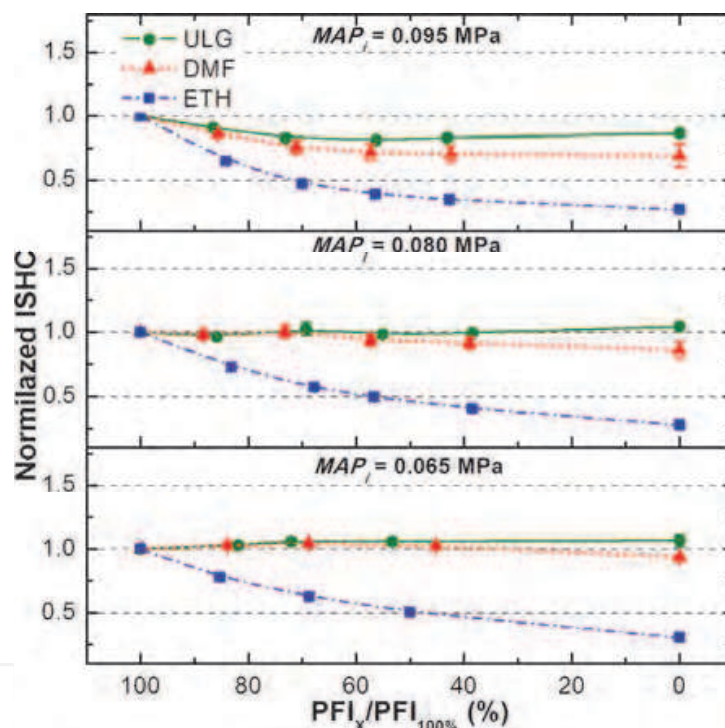


Fig. 28. Normalized Indicated Specific Hydrocarbon Emissions to 100% PFI condition with reduced mass fractions of PFI fuelling using Gasoline, DMF and Ethanol

Figure 29 shows the trend in the normalized indicated specific  $\text{NO}_x$  (is $\text{NO}_x$ ) emissions between the three fuels. The  $\text{NO}_x$  emissions are related to the fuel type. For the same excess air ratio, the nitric oxide or NO emissions, which represent the majority of  $\text{NO}_x$  emissions, decrease with increasing H:C ratio (Harrington 1973). For the three fuel candidates, the H:C ratio increases in the order of DMF, gasoline, and then ethanol. Thus, the  $\text{NO}_x$  emissions should reflect this order based on the pure fuel test results. As shown in Figure 29, the is $\text{NO}_x$  emissions are in the decreasing order of DMF, gasoline, and ethanol, which reflects the H:C ratio order and generally agrees with previous results. In terms of fuel delivery, when reducing the PFI proportion and thus increasing the DI proportion, the charge-cooling effect is increased, which decreases the in-cylinder temperature and helps to suppress  $\text{NO}_x$ .

formation. This effect is clearly shown when substituting gasoline from PFI to DI. Although this decrease is moderate for gasoline, it is much more obvious than for ethanol. Ethanol has a higher heat of vaporization and lower stoichimetric air-fuel ratio. Thus, the charge-cooling effect is much more prominent when using ethanol.

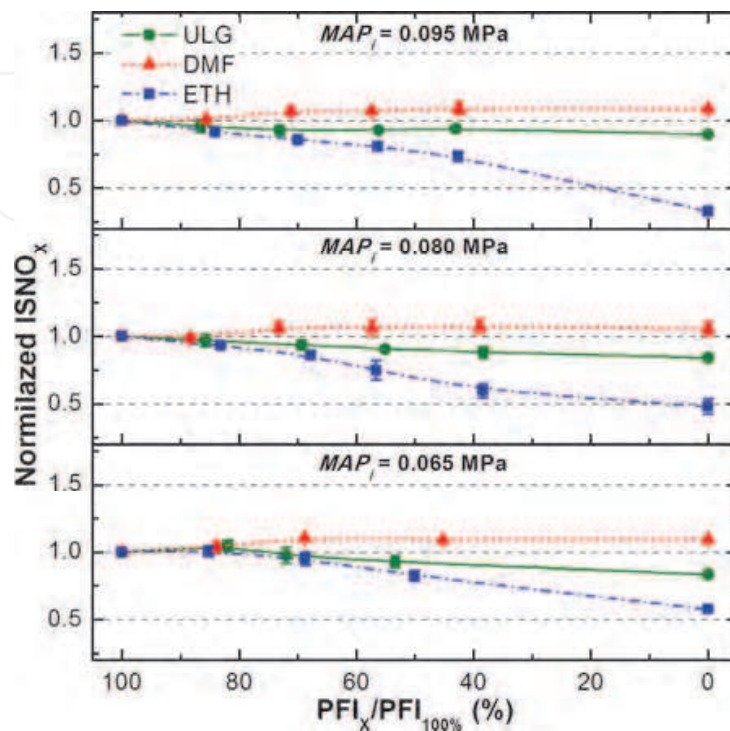


Fig. 29. Normalized Indicated Specific NO<sub>x</sub> Emissions to 100% PFI condition with reduced mass fractions of PFI fuelling using Gasoline, DMF and Ethanol

Figure 30 shows the normalized indicated specific carbon dioxide (isCO<sub>2</sub>) emissions. Carbon dioxide is a non-toxic gas and is not classified as a pollutant engine emission. However, in recent years, the monitoring of CO<sub>2</sub> emissions has become more critical because it is considered to contribute to global temperature rises. Thus, the normalized isCO<sub>2</sub> emissions are highlighted. For gasoline, the dual-injection strategy helps to reduce the isCO<sub>2</sub> emissions at each MAP<sub>i</sub>. The CO<sub>2</sub> emissions give an indication of the combustion efficiency and have been shown to decrease when switching from PFI to DI. The drop in efficiency helps to explain the reduction in isCO<sub>2</sub> emissions when using only gasoline. The H:C ratio also affects the CO<sub>2</sub> emissions concentration. Therefore, although ethanol has the highest H:C ratio, which helps to reduce the isCO<sub>2</sub> emissions, the relatively larger increase in IMEP compromises this benefit. This explains the similar isCO<sub>2</sub> performance of ethanol and gasoline. When using DMF in DI, the isCO<sub>2</sub> emissions increase at each MAP<sub>i</sub>. This increase is mainly due to the lower H:C ratio. However, as a biofuel candidate, the lifecycle CO<sub>2</sub> emissions for DMF must be considered. DMF consumes CO<sub>2</sub> in its production stage, which would help to offset the increase in the engine-out CO<sub>2</sub> emissions.

In summary, this section has introduced a novel approach for utilizing biofuels in modern spark-ignition engines. The application of the dual-injection system is obviously beneficial despite a potential increase in cost. The engine power output increases with direct-injection substitution regardless of the alternative fuel used. We believe that, with more careful optimisation of injection and spark timing, the drop in efficiency and increases in NO<sub>x</sub> and



CO<sub>2</sub> emissions will be compensated for. Nevertheless, the reduction in HC emissions and attraction of blend ratio control and optimisation highlights the benefit of the dual-injection strategy with such biofuels as ethanol and DMF.

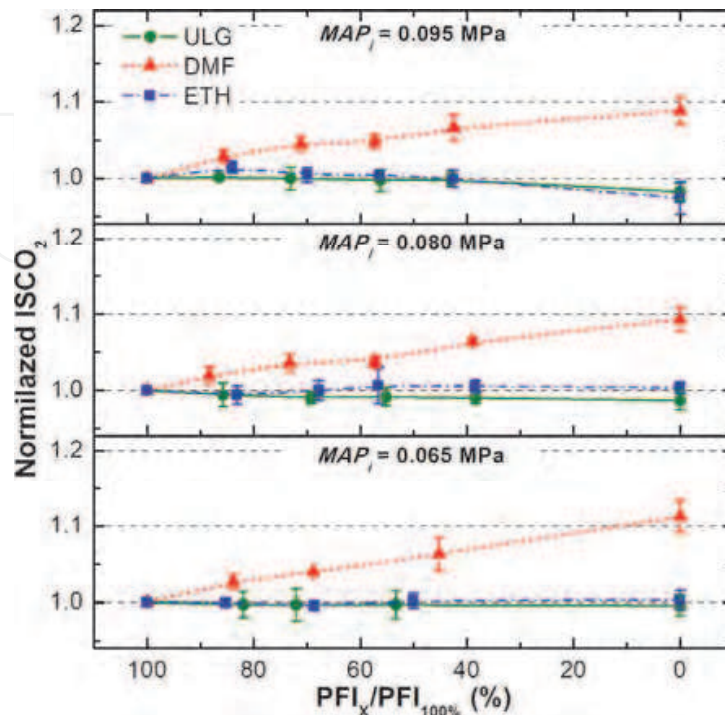


Fig. 30. Normalized Indicated Specific Carbon Dioxide Emissions to 100% PFI condition with reduced mass fractions of PFI fuelling using Gasoline, DMF and Ethanol

## 8. Summary

In this chapter, we introduced 2,5-dimethylfuran, a newly recognised and potential biomass-derived alternative fuel for spark-ignition engines. Initial tests have included the fundamental combustion and spray analysis, basic engine tests to examine the effect on the engine performance and regulated emissions and further, more detailed unregulated emissions analysis, including particulate emissions. The chapter concludes with a new approach for the improved utilisation of biofuels and is referred to as the dual-injection system.

The results show how DMF is a promising alternative fuel. It has very similar properties to gasoline with regards to combustion, which means that it can be easily adopted with current spark-ignition engine technologies without the need for major modifications. Compared to the other major gasoline-alternative biofuel, ethanol, DMF is marginally inferior in terms of its laminar burning velocity, engine efficiency and engine-out emissions. However, since these emissions are nowadays combated by very effective aftertreatment systems, the advantages of DMF's higher energy density and potentially better cold-start performance are evident. Furthermore, the production of DMF does not compete with food and so makes it an attractive option.

The PM emissions of DMF (currently an unregulated requirement in Europe and the US) have been shown to be comparable to that of gasoline at low load. This work is ongoing and further results are likely to follow in publications by the authors, including an investigation

of the individual hydrocarbons. Such results will show details of the toxic compounds and help to better understand the potential effect on the environment and to human health.

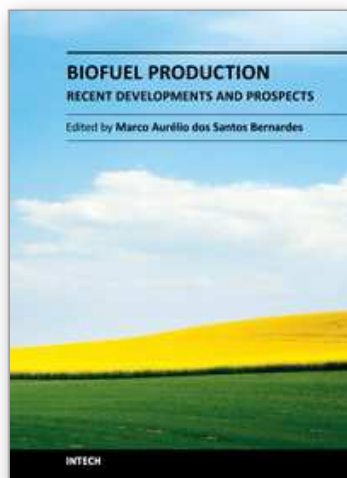
Finally, the dual-injection strategy offers an efficient and flexible use of biofuels, whilst still using gasoline. It offers the high engine performance of a modern DI system, the low NO<sub>x</sub>, CO<sub>2</sub> and HC emissions of a PFI system and the possibility to run the engine using any blend ratio with limited implications to hardware cost.

## 9. Acknowledgement

The authors of this chapter would like to acknowledge the support from Jaguar Cars Ltd, Shell Global Solutions and various research assistants and technicians at the University of Birmingham, UK. They would also like to acknowledge the support from their international collaborators at Tsinghua University, China and Xuesong Wu from Xi'an Jiaotong University, China for his help with the dual-injection system.

## 10. Reference

- Bechtold, J. K., Matalon, M. (2001). "The Dependence of the Markstein Length on Stoichiometry." *Combustion and Flame* 127: 1906-1913.
- Chu, C.-C. C. (1986). One-Dimensional Transient Fluid Model for Fuel-Coolant Interaction Analysis, University of Wisconsin-Madison. PhD Thesis.
- Bradley, D., Hicks, R.A., Lawes, M., Sheppard, C.G.W. and Woolley, R. (1998). "The Measurement of Laminar Burning Velocities and Markstein Numbers for Iso-octane-Air and Iso-octane-n-Heptane-Air Mixtures at Elevated Temperatures and Pressures in an Explosion Bomb." *Combustion and Flame* 115: 126-144.
- Gautam, M. and Martin, D.W. (2000). "Combustion characteristics of higher-alcohol/gasoline blends." *IMEchE* 214: 497-511.
- Harrington, J.A. and Shishu, R.C. (1973). "A Single-Cylinder Engine Study of the Effects of Fuel Type, Fuel Stoichiometry, and Hydrogen-to-Carbon Ratio and CO, NO, and HC Exhaust Emissions." SAE 730476.
- Heywood, J. B. (1988). *Internal Combustion Engine Fundamentals*, McGraw-Hill.
- Law, C. K. (2006). *Combustion Physics*, Cambridge University Press.
- Luque, R., Herrero-Davila, L., Campelo, J.M., Clark, J.H, Hidalgo, J.M., Luna, D., Marinasa, J.M. and Romeroa, A.A. (2008). "Biofuels: a technological perspective." *Energy & Environmental Science* 1: 542-564.
- Mascal, M. and Nikitin, E.B. (2008). "Direct High-Yield Conversion of Cellulose into Biofuel." *Angewandte Chemie International Edition* 47: 7924-7926.
- Stone, R. (1999). *Introduction to Internal Combustion Engines*, Basingstoke: Macmillan Press Ltd.
- Wu, X., Huang, Z. and Jin, C. (2009). "Measurements of Laminar Burning Velocities and Markstein Lengths of 2,5-Dimethylfuran-Air-Diluent Premixed Flames." *Energy and Fuels* 23: 4355-4362.
- Roman-Leshkov, R., Barrett, C.J., Liu, Z.Y. and Dumesic, J.A. (2007). "Production of dimethylfuran for liquid fuels from biomass-derived carbohydrates." *Nature* 447: 982-986.
- Zhao, F., Lai, M.C. and Harrington, D.L. (1999). "Automotive spark-ignited direct-injection gasoline engines." *Prog. Energy Combust. Sci.* 25(5): 437-562.
- Zhao, H., Holladay, J.E., Brown, H. and Zhang, Z.C. (2007). "Metal Chlorides in Ionic Liquid Solvents Convert Sugars to 5-Hydroxymethylfuran." *Science* 5831: 1597-1600.



## **Biofuel Production-Recent Developments and Prospects**

Edited by Dr. Marco Aurelio Dos Santos Bernardes

ISBN 978-953-307-478-8

Hard cover, 596 pages

**Publisher** InTech

**Published online** 15, September, 2011

**Published in print edition** September, 2011

This book aspires to be a comprehensive summary of current biofuels issues and thereby contribute to the understanding of this important topic. Readers will find themes including biofuels development efforts, their implications for the food industry, current and future biofuels crops, the successful Brazilian ethanol program, insights of the first, second, third and fourth biofuel generations, advanced biofuel production techniques, related waste treatment, emissions and environmental impacts, water consumption, produced allergens and toxins. Additionally, the biofuel policy discussion is expected to be continuing in the foreseeable future and the reading of the biofuels features dealt with in this book, are recommended for anyone interested in understanding this diverse and developing theme.

### **How to reference**

In order to correctly reference this scholarly work, feel free to copy and paste the following:

Guohong Tian, Ritchie Daniel and Hongming Xu (2011). DMF - A New Biofuel Candidate, Biofuel Production-Recent Developments and Prospects, Dr. Marco Aurelio Dos Santos Bernardes (Ed.), ISBN: 978-953-307-478-8, InTech, Available from: <http://www.intechopen.com/books/biofuel-production-recent-developments-and-prospects/dmf-a-new-biofuel-candidate>

**INTECH**  
open science | open minds

### **InTech Europe**

University Campus STeP Ri  
Slavka Krautzeka 83/A  
51000 Rijeka, Croatia  
Phone: +385 (51) 770 447  
Fax: +385 (51) 686 166  
[www.intechopen.com](http://www.intechopen.com)

### **InTech China**

Unit 405, Office Block, Hotel Equatorial Shanghai  
No.65, Yan An Road (West), Shanghai, 200040, China  
中国上海市延安西路65号上海国际贵都大饭店办公楼405单元  
Phone: +86-21-62489820  
Fax: +86-21-62489821

© 2011 The Author(s). Licensee IntechOpen. This chapter is distributed under the terms of the [Creative Commons Attribution-NonCommercial-ShareAlike-3.0 License](https://creativecommons.org/licenses/by-nc-sa/3.0/), which permits use, distribution and reproduction for non-commercial purposes, provided the original is properly cited and derivative works building on this content are distributed under the same license.

IntechOpen

IntechOpen